AIChE

Operational Modeling of Multistream Heat Exchangers with Phase Changes

M. M. Faruque Hasan and I. A. Karimi
Dept. of Chemical and Biomolecular Engineering, National University of Singapore, Engineering Drive 4, Singapore 117576

H. E. Alfadala
Dept. of Chemical Engineering, Qatar University, P.O. Box 2713, Doha, Qatar

H. Grootjans
Qatargas Operating Company, Ltd., P.O. Box 22666, Doha, Qatar

DOI 10.1002/aic.11682
Published online December 4, 2008 in Wiley InterScience (www.interscience.wiley.com).

Multistream heat exchangers (MSHE) enable the simultaneous exchange of heat among multiple streams, and are preferred in cryogenic processes such as air separation and LNG. Most MSHEs are complex; proprietary and involve phase changes of mixtures. Although modeling MSHE is crucial for process optimization, no such work exists to our knowledge. We present a novel approach for deriving an approximate operational (vs. design) model from historic data for an MSHE. Using a superstructure of simple 2-stream exchangers, we propose a mixed-integer nonlinear programming (MINLP) formulation to obtain a HE network that best represents the MSHE operation. We also develop an iterative algorithm to solve the large and nonconvex MINLP model in reasonable time, as existing commercial solvers fail to do so. Finally, we demonstrate the application of our work on an MSHE from an existing LNG plant, and successfully predict its performance over a variety of seasons and feed conditions.
© 2008 American Institute of Chemical Engineers *AIChE J,* 55: 150–171, 2009
Keywords: multi-stream heat exchangers, phase change, cryogenics, main cryogenic heat exchanger, superstructure, MINLP, LNG

Introduction

A multistream heat exchanger (MSHE) is a single unit in which multiple hot and cold streams exchange heat simultaneously. Plate & fin, spiral-wound, and multipass shell and tube are the most common types of MSHEs. Many MSHEs use several sections (called bundles) in a series (Figure 1).[1] For instance, a spiral-wound MSHE has multiple bundles, and each bundle has several concentric rows of tubes that are spirally wound around the central axis of its shell. Normally, a low-pressure refrigerant such as a pure or multicomponent refrigerant flows down the shell side passing through all the bundles in the series. Multiple high-pressure hot streams may enter each bundle, and they flow in separate concentric sets of tubes. Thus, the heat exchange between the shell-side cold fluid and tube-side hot streams is more-or-less crosscurrent.

Most MSHEs are proprietary, and their compact and complex designs enable reductions in materials of construction, piping and supporting structures, weight, and space. They offer high-flexibility in the flow arrangement, which in turn minimizes the heat-transfer area. They are usually associated with large heat transfer at temperature differences as small as 1–3 $^{\circ}C$[2] at the cold ends to enhance efficiency.[3] The distinguishing features of MSHEs include the presence of a large

Correspondence concerning this article should be addressed to I. A. Karimi at cheiak@nus.edu.sg.

© 2008 American Institute of Chemical Engineers

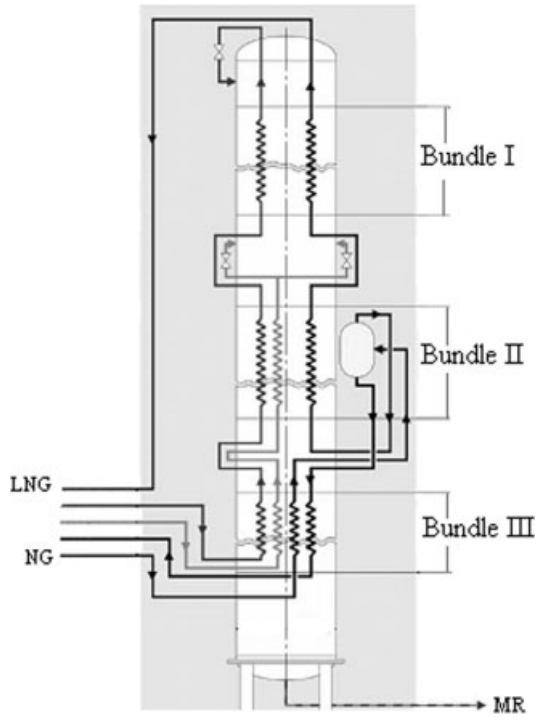

Figure 1. Schematic of an industrial MSHE from Linde.

number of passages or channels,[3] complex heat-transfer paths,[4] high heat transfer coefficients, high-density of heat-transfer area, and capability to withstand a range of pressures, high-reliability, and minimum maintenance.

Due to their safe and cost-effective designs and the need for higher effectiveness and efficiency,[3] MSHEs are extremely popular in many energy-intensive industrial and cryogenic processes including air separation/liquefaction, natural gas processing, liquid hydrogen, petrochemicals, and liquefied natural gas (LNG). Although brazed aluminum plate & fin heat exchangers (HEs) are popular in many cryogenic applications, spiral-wound HEs are also equally common, especially as the main cryogenic heat exchangers (MCHEs) in the LNG industry. They are critical in offshore and marine industry applications such as Floating Production Storage & Offloading units (FPSOs) for stranded LNG, since space is at a premium. Some MSHEs serve multiple purposes. For example, reversing exchangers[3] with cyclical changeover of one stream in air separation plants also remove impurities in a continuous operation.

Conceptually[5,6] it is possible for a single MSHE to replace an entire heat exchanger network (HEN) of single-hot-single-cold or 2-stream HEs. Thus, the application of MSHEs is clearly not limited to subambient processes only, and MSHEs may offer an attractive option in improving the energy performance of a chemical plant. This becomes especially true, as energy costs are rising. For instance, energy accounts for as much as 40% of the total operating cost[7] of a plant. A world-scale base-load* LNG plant, having a capacity exceeding 2.5 mtpa (million tonnes per annum) through one train, consumes about 5.5-6.0 kWh per kmol of LNG.[8]

Developing efficient and accurate models to predict and/or optimize MSHE operation is an inevitable first step toward system-wide optimization. To illustrate the need of such models, consider an LNG plant, which is essentially a huge and highly energy-intensive condenser that requires refrigeration. MCHE (Figure 1) is at the heart of this refrigeration, which produces and subcools LNG to around -150 °C. The refrigeration section is the largest consumer of energy in an LNG plant, and the overall efficiency of an LNG plant depends largely on the MCHE performance that can vary considerably with changes in feed, operating, and ambient conditions. Most deviations from normal operation in an LNG plant are mitigated by changing the MCHE operation. For example, during summer, when the ambient temperature is high, and the gas turbines are operating at maximum available power, the plant operators change several parameters such as refrigerant composition, MCHE pressure, LNG temperature at the MCHE outlet, natural gas feed rate, etc. However, these changes are mostly based on experience alone, and may lead to inefficient operation and capacity reduction. A rigorous and predictive model for an MSHE such as the MCHE would help reduce the guesswork and trial-and-error in plant operation. A model validated using plant operational data would enable the operators to predict the possible outcomes of any control action systematically, before actually taking that action. Furthermore, often refrigeration systems are connected in complex ways with MSHEs, and cannot be optimized rigorously without a model for the MSHE. Similarly, MSHEs usually link a plant's upstream and downstream sections, hence a suitable MSHE model is essential for simulating and optimizing a plant.

Most existing literature on improving energy consumption and efficiency uses an exergy analysis[7,9–12] of MSHEs and other equipment in cryogenic plants, since that provides guidelines for efficient energy usage[13] in terms of irreversible losses at different points in the plant. However, reducing exergy losses does not always mean reducing cost.[12] Moreover, since such an analysis focuses mainly on improving the performance of individual pieces of equipment, it may not serve the ultimate goal of plant-wide optimization. Alternate approach is to apply the advanced techniques of process modeling, synthesis, and optimization.[14] Although, the use of such techniques in the gas processing industry is increasing, a major challenge is to develop models that can be solved repeatedly. Lee et al.[2] and Vaidyaraman and Maranas[15] proposed NLP formulations for the synthesis of mixed-refrigerant systems. Recently, Del Nogal et al.[16] presented an optimization framework to integrate refrigeration and power systems, based on a combination of stochastic optimization and MILP formulations.

Most research related to complex HEs focuses on the design to minimize cost and certain operational targets such as pressure drops.[5] While some literature[17,18] has used optimization-based approaches for the optimal design of plate & fin HEs, we are able to locate very few papers[19,20] on spiral-wound HEs. These articles used numerical approaches to perform thermal design. However, all existing work targets design rather than performance rating, and requires the knowledge of internals such as tubes, bundles, flow arrangement, etc. To the

*Base-load plants are those that operate throughout the year with a continuous supply of feed (natural gas), at a rate of 50 to 1,000 MMSCFD or even more. Base-load plants usually have larger capacities than peak-shaving plants.

best of our knowledge, only Hasan et al.[21,22] have modeled MCHE and addressed the operational aspects of an existing MSHE in the open literature. However, their preliminary model did not consider the operational data at different time points, and they did not report any solution algorithm.

The modeling of an MSHE is nontrivial. MSHEs such as those used as cold boxes in air separation plants, and MCHEs designed by Air Products and Linde for LNG plants are proprietary, and their physical details are confidential. Atypical and nonlinear temperature distributions[3] are also common in low-temperature processes, where the heat capacity can vary significantly with temperature. One reason behind this is the presence of phase changes within an MSHE due to the liquefaction and/or evaporation of multicomponent mixtures. For example, in an LNG plant, natural gas (a mixture of methane, ethane, propane, butane, nitrogen, etc.) liquefies in an MCHE. Temperature-enthalpy relations (T-H curve) of such streams are highly nonlinear, and vary significantly from one phase to another. These make the modeling of complex, proprietary, multistream, and multiphase HEs difficult, which can be a bottleneck in optimization studies.

In principle, one could model an MSHE in two ways. One is to use rigorous physicochemical models like computational fluid dynamic models, but such models present a serious problem in optimization, because of their compute-intensive and time-consuming nature. Moreover, this type of modeling is difficult, and even impossible, for almost nothing about the physical details and configuration of many MSHEs are available in the public domain. An alternate approach would be to develop a simpler model that can predict the performance of an existing MSHE without knowing its physical details, but using operational data only. This is what we intend to do in this article. The advantage of this type of modeling is that it can be embedded in an optimization model.

In this article, we develop a novel model for MSHEs to predict their operational performance based on operational data. This work is inspired by a real need in and keen interest from base-load LNG plants. The modeling approach presented here is independent of the MSHE type (plate & fin, spiral-wound, and multipass shell & tube), and does not require any information about the internals. The generality of our model also allows the modeling of MSHEs from any process, ambient or cryogenic, and onshore or offshore.

The remainder of this article is organized as follows. First, we present the problem statement. We then present the modeling concept and describe the MINLP formulation for the operational modeling of MSHEs with phase change. We then discuss an efficient solution strategy to solve large models within reasonable time, which commercial solvers fail to solve. Finally, to illustrate the applicability of our approach, we present a case study for an existing MCHE from an LNG plant, for which we develop a predictive model and verify its ability to predict future performance.

Problem Statement

Consider the steady state operation of an MSHE under various scenarios (ambient temperatures, feed conditions, etc.). For each such scenario, we gather representative operational data (temperatures, pressures, flow, etc.). We use n as the index to denote various such data sets. For simplicity, we focus on one single bundle, as the treatment is identical for all bundles. Let i ($i = 1, 2, \ldots, I$) denote I hot streams entering the bundle. Let M_i^n be the molar flow rate, and TIN_i^n and $TOUT_i^n$ be the inlet and outlet temperatures, respectively, of stream i for that bundle in the data set n. The refrigerant is a mixture of several components. For instance, the refrigerant in LNG industry, usually known as mixed refrigerant, is a mixture of methane, ethane, propane, butane, and nitrogen. From now on, we call it MR. Let M_{MR}^n denote the molar flow rate, and TIN_{MR}^n and $TOUT_{MR}^n$ denote the inlet and outlet temperatures, respectively, of the MR in the same data set. Given these and other operational data such as pressures and compositions of all streams over N data sets ($n = 1, 2, \ldots, N$), we wish to obtain (1) a network configuration of 2-stream HEs, which best describes the operation of the MSHE, (2) heat-transfer area of each HE in the network, and (3) the portion of MR that passes through each HE.

MINLP Formulation

Our main idea is to view an MSHE, as if it were a network of simple 2-stream HEs with known heat-transfer areas. Each 2-stream HE will exchange heat between one of the hot streams and a portion MR. The network would involve substreams of the same process streams, and perform the same duties that an actual MSHE does, but it would not have an exact resemblance to the actual physical details of the MSHE. To arrive at such a network, we exploit the concept of superstructure that would allow any configuration involving mixing and/or splitting of streams, and all possible matches between hot and cold streams. We expect that optimization using such a superstructure would yield the best network representing the actual operation of the MSHE.

It is worth comparing our aforementioned modeling approach with the usual HE network synthesis (HENS) approach from the literature. In the conventional HENS approach, hot streams are to be cooled, and cold streams are to be heated to specific temperatures by either exchanging heat among themselves using 1-1 matches, or using process utilities. Excellent reviews on HENS are available in Gundersen and Naess[23] and Furman and Sahinidis.[24] However, unlike the HENS problem, our modeling of MSHE is not a design problem. Moreover, it involves complete heat integration between hot streams and MR. Therefore, it does not require other hot (e.g., steam) and cold (e.g., cooling water) process utilities. Our goal is to derive a network of 2-stream HEs using the real operational data (in/out temperatures, pressures, flow rates, etc.) of a MSHE to enable the prediction of future performance. Data that cover operation over a variety of seasons and feed conditions will be used to obtain a network for the MSHE, so that its performance can be described or predicted over a wide range of operating and environmental conditions. While we agree that this article deals with phase changes in the context of the operational modeling of MSHEs, it also provides the first step toward doing the same in the context of heat integration. In fact, we have just finished that extension and will report it in near future.

As the first step, we develop the superstructure of HEs that would form the basis for our HE network. Based on the stagewise superstructure representation of Yee et al.,[6] Yee

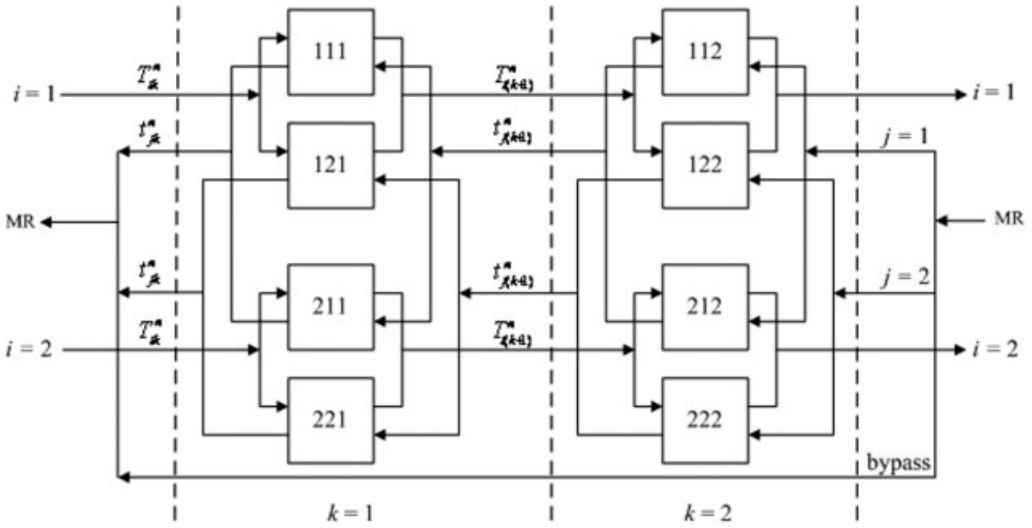

Figure 2. Superstructure for a bundle of MCHE.

and Grossmann[25] proposed a superstructure comprising multiple stages, where each stage allows every pairwise exchange between hot and cold streams in a countercurrent fashion. However, they did not allow stream bypass. Ciric and Floudas[26] also addressed a similar HENS problem, and modeled it as an MINLP problem. In this work, we use a modified version of stagewise superstructure that allows bypass of MR.

Let I hot streams ($i = 1, 2, \ldots, I$) with mass flows M_i^n enter the tube side of a bundle. Because these streams flow in separate sets of concentric tubes in a spiral-wound HE, or through separate plates in a plate & fin HE to form individual flow passages,[3] we do not allow heat exchange between any two hot streams in our model. The flow of MR along the bundle axis and across the bundle's concentric sets of tubes is complex. When MR enters the bundle, it normally passes through a distribution system[1] to reduce channeling and ensure better heat transfer. Therefore, we split MR into some known J cold streams ($j = 1, 2, \ldots, J$) of unknown flows that remain constant throughout the bundle. We achieve this by defining an unknown split fraction f_j of cold stream j, which is a variable in our optimization formulation, such that the mass flow of cold stream j through the bundle for data set n is $f_j M_{MR}^n$. Note that f_j is independent of data sets, as it is meant to model the physical flow pattern of MR in a bundle. In addition to describing the flow reality more accurately, this splitting also helps in obtaining a network with better accuracy vs. that using one single cold stream (MR). The use of one single cold stream forces the temperature driving forces to decrease considerably along the axis, and requires prioritization of hot streams for heat exchange. This results in more complex network and larger heat-transfer areas in later stages of the superstructure. However, we still need to select an appropriate J. While a large J may increase the size of the superstructure considerably, we should select J such that each hot stream has a chance to exchange heat in every stage of the superstructure. Therefore, $J \geq I$ would be desirable, and we set $J = I$ in this work. Let the superstructure has K stages ($k = 1, 2, \ldots, K$). Following Yee et al.,[6] we set $K = \max[I, J]$ in this work. For the data set n, we define $T_{ik}^n (T_i^{n,L} \leq T_{ik}^n \leq TIN_i^n)$ and $t_{j(k+1)}^n (TIN_{MR}^n \leq t_{j(k+1)}^n \leq t_{MR}^{n,U})$ as the temperatures at which hot stream i and cold stream j enter stage k, respectively. Note that $T_{i1}^n = TIN_i^n$ and $t_{j(K+1)}^n = TIN_{MR}^n$ are known data, and we set some reasonable but conservative values for $T_i^{n,L}$ and $t_{MR}^{n,U}$.

Using the aforementioned approach, Figure 2 shows a superstructure for a bundle with $I = 2$, $J = 2$, and $K = 2$. In addition to the J cold streams, we have shown one bypass stream for MR as an option for channeling or bypassing excess MR, which usually occurs in practice. The rectangles in Figure 2 represent HEs indexed by (i, j, k). For instance, HE 121 refers to the exchanger where hot stream ($i = 1$) contacts cold stream ($j = 2$) at stage ($k = 1$).

As stated earlier, MSHEs normally involve multicomponent phase changes. A typical constant-pressure T-H curve for a mixture has three distinct regions partitioned by its bubble- and dew-point temperatures (BPT and DPT). The nature of this T-H curve varies significantly from one region to another as shown in Figure 3 for different mixtures. In contrast to T $\geq$ DPT and T $\leq$ BPT, where straight lines can be reasonable approximations, the T-H curves for most mixtures are nonlinear in the range BPT $<$ T $<$ DPT. While isothermal phase changes are addressed in HENS,[27] nonlinear T-H curves are not rigorously modeled. Recently, Hasan et al..[21,22] modeled MCHE with multicomponent phase change, and then extended the approach to generalize current HENS[28] work.

In this work, we make the following assumptions:

1. Hot streams supply heat to MR only. No heat transfer between hot streams is allowed.

2. For each data set, the stream compositions, pressures, DPTs, and BPTs are all known constants through the entire bundle.

3. All inlet and outlet temperatures in the data sets are the actual inlet and outlet temperatures of the streams in the MSHE bundle.

4. The film heat-transfer coefficient h_i^n for a hot stream i in data set n is given[29,30] by $h_i^n = \alpha_i \left(M_i^n\right)^{0.8}$, where α_i is a parameter that depends on fluid and exchanger properties.

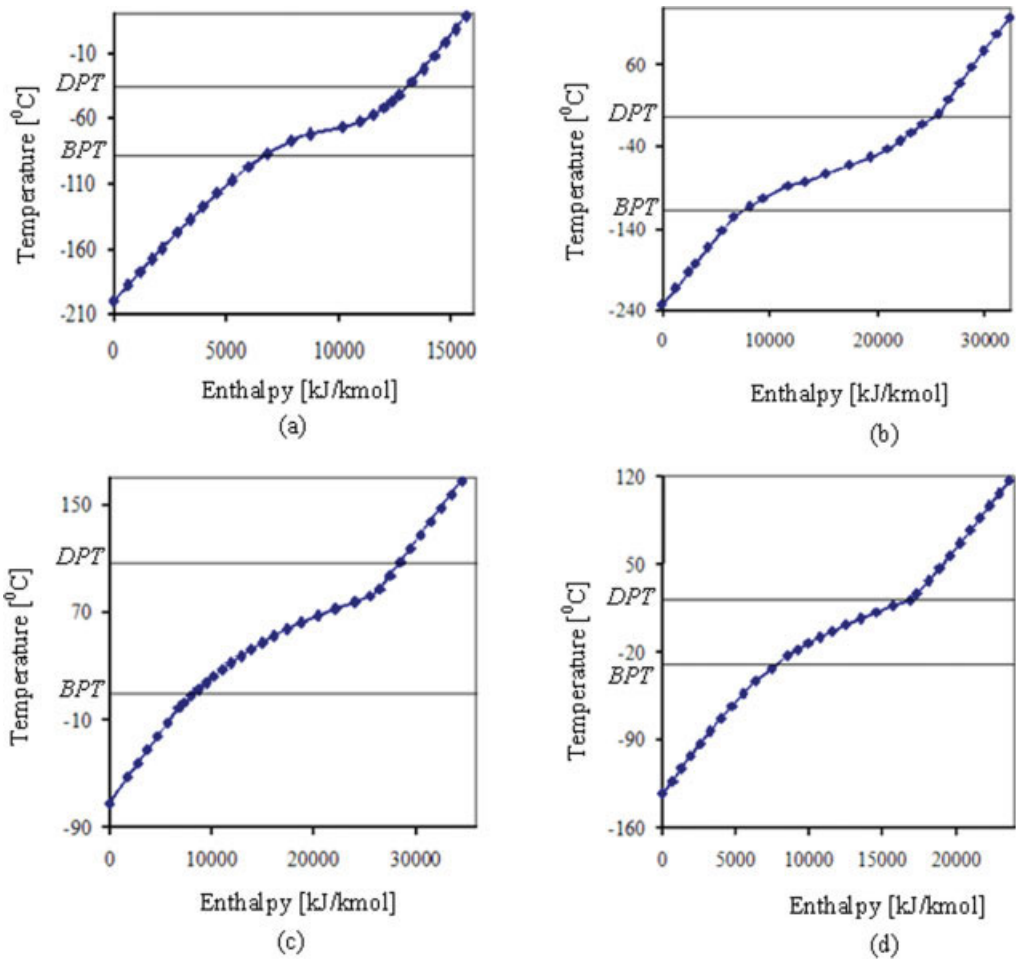

Figure 3. Temperature-enthalpy relations for different mixtures.

[Color figure can be viewed in the online issue, which is available at www.interscience.wiley.com.]

5. The film heat-transfer coefficient h_j^n for a cold stream j in data set n is given[31,32] by $h_j^n = \beta\left(f_j M_{MR}^n\right)^{0.25}$, where β is a parameter that depends on fluid and exchanger properties.

6. Fouling and other thermal resistances are negligible, and the overall heat-transfer coefficient is given by

$$U_{ij}^n = \frac{\alpha_i \beta \left(M_i^n\right)^{0.8} \left(f_j M_{MR}^n\right)^{0.25}}{\alpha_i \left(M_i^n\right)^{0.8} + \beta \left(f_j M_{MR}^n\right)^{0.25}}$$

which is a function of f_j only.

With the aforementioned discussion, we now present an MINLP formulation for deriving the best network of HEs describing a given bundle. Unless stated otherwise, all indices such as i, j, k, n, etc., assume the full ranges of their valid values in all the constraints.

Our model involves two primary decisions. One concerns the distribution of MR across the bundle, as modeled by split fraction. As stated earlier, the MR flow is split into J cold streams with unknown split fractions. Allowing for the channeling of MR in a real operation, we must have

$$\sum_{j=1}^{J} f_j \leq 1 \tag{1}$$

Note that given any set of values of f_j, $j < J$, we can always reindex them, such that the following equation is satisfied

$$f_j \geq f_{j+1} \qquad j < J \tag{2}$$

Equation 2 causes no loss of generality and eliminates redundant combinations of f_j.

The other primary decision is to select appropriate matches between hot and cold streams. To model the existence of a HE between hot stream i and cold stream j at stage k, we define a binary variable x_{ijk} for $i = 1, 2, \ldots, I$, and $j = 1, 2, \ldots, J$

$$x_{ijk} = \begin{cases} 1 & \text{if a HE exists between a hot stream } i \text{ and a cold stream } j \text{ at stage } k \\ 0 & \text{otherwise} \end{cases}$$

Note that both the primary decisions do not involve the data set index n. As mentioned earlier, hot streams flow in separate sets of plates or concentric tubes inside the bundle. Therefore, we assume that each hot stream contacts only one cold stream at each stage and vice versa. This resembles the

"no stream splitting" assumption used by Yee and Grossmann[25] at each stage in the superstructure. Thus

$$\sum_j x_{ijk} \le 1 \tag{3}$$

$$\sum_i x_{ijk} \le 1 \tag{4}$$

Furthermore, to prevent a repeat heat exchange between the same hot and cold streams in two consecutive stages, we use

$$x_{ijk} + x_{ij(k+1)} \le 1 \tag{5}$$

Because all hot streams get cooled, at least one HE must exist for each hot stream i.

$$\sum_j \sum_k x_{ijk} \ge 1 \tag{6}$$

Now, a hot (cold) stream i (j) with a temperature $T^n_{ik}(t^n_{jk})$ must be in one of three states, namely gas, liquid, or 2-phase. We define these three states as follows

$s = 1$: $T^n_{ik} \ge DPT^n_i (t^n_{jk} \ge DPT^n_{MR})$ (gaseous state)

$s = 2$: $BPT^n_i \le T^n_{ik} \le DPT^n_i (BPT^n_{MR} \le t^n_{jk} \le DPT^n_{MR})$ (2-phase state)

$s = 3$: $T^n_{ik} \le BPT^n_i (t^n_{jk} \le BPT^n_{MR})$ (liquid state)

Note that the direction of state-change is opposite for hot and cold streams. Now, to identify the state in which a stream enters a stage k, we define the following binary variables

$$Y^n_{iks} = \left\{ \begin{array}{ll} 1 & \text{if a hot stream } i \text{ enters a stage} \\ & \quad k \text{ in a state } s \text{ for data set } n \\ 0 & \text{otherwise} \end{array} \right\}$$

$$y^n_{j(k+1)s} = \left\{ \begin{array}{ll} 1 & \text{if a cold stream } j \text{ enters a stage } k \\ & \quad \text{in a state } s \text{ for data set } n \\ 0 & \text{otherwise} \end{array} \right\}$$

Y^n_{iks} and $Y^n_{i(k+1)s}$ ($y^n_{j(k+1)s}$ and y^n_{jks}) represent the states of a hot (cold) stream i (j), as it enters and leaves a stage k respectively. Note that since $T^n_{i1} = TIN^n_i$ and $t^n_{j(K+1)} = TIN^n_{MR}$ are known, Y^n_{i1s} and $y^n_{j(K+1)s}$ are known constants. Clearly, a stream can enter a stage in only one state. Therefore

$$\sum_s Y^n_{iks} = \sum_s y^n_{jks} = 1 \tag{7a,b}$$

If a hot stream i enters a stage $(k + 1)$ in the gaseous state (i.e., $Y^n_{i(k+1)1} = 1$), then it must enter all other previous stages in the gaseous state also. In other words

$$Y^n_{ik1} \ge Y^n_{i(k+1)1} \tag{8a}$$

Similarly, if a cold stream j enters a stage k in the gaseous state (i.e., $y^n_{j(k+1)1} = 1$), then it must enter all the stages lower than k in the gaseous state also. In other words

$$y^n_{jk1} \ge y^n_{j(k+1)1} \tag{8b}$$

Following the same argument for the liquid state, we have

$$Y^n_{i(k+1)3} \ge Y^n_{ik3} \tag{9a}$$

$$y^n_{j(k+1)3} \ge y^n_{jk3} \tag{9b}$$

It also follows that if a hot stream leaves a stage k in the 2-phase state (i.e., $Y^n_{i(k+1)2} = 1$), then it must leave all previous stages either in the 2-phase state or in the gaseous state. Therefore

$$Y^n_{ik1} + Y^n_{ik2} \ge Y^n_{i(k+1)2}$$

Similarly, if a hot stream enters a stage k in the 2-phase state (i.e., $Y^n_{ik2} = 1$), then it must leave the stage either in the 2-phase state or in the liquid state. This implies

$$Y^n_{i(k+1)2} + Y^n_{i(k+1)3} \ge Y^n_{ik2}$$

However, the last two constraints can be derived from Eqs. 7–9, and, hence, are redundant (proof in Appendix A). A similar argument rules out the presence of such constraints for cold streams.

Lastly, if no HE exists for a stream in a stage, then the stream must enter and exit the stage in the same state. Therefore

$$\sum_j x_{ijk} \ge Y^n_{iks} - Y^n_{i(k+1)s} \qquad \text{for } s = 1, 2 \tag{10a}$$

$$\sum_j x_{ijk} \ge Y^n_{i(k+1)s} - Y^n_{iks} \qquad \text{for } s = 2, 3 \tag{11a}$$

$$\sum_i x_{ijk} \ge y^n_{jks} - y^n_{j(k+1)s} \qquad \text{for } s = 1, 2 \tag{10b}$$

$$\sum_i x_{ijk} \ge y^n_{j(k+1)s} - y^n_{jks} \qquad \text{for } s = 2, 3 \tag{11b}$$

Temperature Changes across Three States

We distribute the total temperature change $[= T^n_{ik} - T^n_{ik+1}(t^n_{jk} - t^n_{jk+1})]$ at a stage k for a hot (cold) stream across the three states s = 1–3 by defining $\Delta T^n_{iks} \ge 0 (\Delta t^n_{jks} \ge 0)$ as the portion of the temperature change that occurs in state s of hot (cold) stream i (j) for data set n (Figure 4). Thus, the total temperature change for a hot (cold) stream i (j) in stage k is given by

$$T^n_{ik} - T^n_{i(k+1)} = \sum_s \Delta T^n_{iks} \tag{12a}$$

$$t^n_{jk} - t^n_{j(k+1)} = \sum_s \Delta t^n_{jks} \tag{12b}$$

A stream (hot or cold) in any stage could have one or more states. However, only the following scenarios for entrance and exit states are possible for a hot (cold) stream i (j).

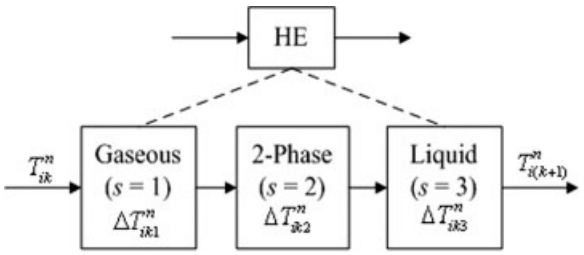

Figure 4. Temperature changes across each state.

1. Gas to gas: $Y^n_{ik1} = Y^n_{i(k+1)1} = 1 (y^n_{j(k+1)1} = y^n_{jk1} = 1)$
2. Liquid to liquid: $Y^n_{ik3} = Y^n_{i(k+1)3} = 1 (y^n_{j(k+1)3} = y^n_{jk3} = 1)$
3. 2-phase to 2-phase: $Y^n_{ik2} = Y^n_{i(k+1)2} = 1 (y^n_{j(k+1)2} = y^n_{jk2} = 1)$
4. Gas to 2-phase (hot streams only): $Y^n_{ik1} = Y^n_{i(k+1)2} = 1$
5. Gas to liquid (hot streams only): $Y^n_{ik1} = Y^n_{i(k+1)3} = 1$
6. 2-phase to liquid (hot streams only): $Y^n_{ik2} = Y^n_{i(k+1)3} = 1$
7. 2-phase to gas (cold streams only): $y^n_{j(k+1)2} = y^n_{jk1} = 1$
8. Liquid to gas (cold streams only): $y^n_{j(k+1)3} = y^n_{jk1} = 1$
9. Liquid to 2-phase (cold streams only): $y^n_{j(k+1)3} = y^n_{jk2} = 1$

Furthermore, the temperature changes in various states must be limited for each scenario. To enforce these limits, we define the following and then consider each scenario separately

$$\Theta^n_{i1} = \max\left[0, TIN^n_i - DPT^n_i\right]$$

$$\Theta^n_{i2} = \max\left[0, \min\left(TIN^n_i, DPT^n_i\right) - BPT^n_i\right]$$

$$\Theta^n_{i3} = \min\left[TIN^n_i, BPT^n_i\right] - \min\left[T^{n,L}_i, BPT^n_i\right]$$

$$\theta^n_1 = \max\left[t^{n,U}_{MR}, DPT^n_{MR}\right] - \max\left[TIN^n_{MR}, DPT^n_{MR}\right]$$

$$\theta^n_2 = \max\left[0, DPT^n_{MR} - \max\left(TIN^n_{MR}, BPT^n_{MR}\right)\right]$$

$$\theta^n_3 = \max\left[0, BPT^n_{MR} - TIN^n_{MR}\right]$$

For scenario 1 (gas-to-gas), Eq. 8a forces $Y^n_{ik1} = 1$, because $Y^n_{i(k+1)1} = 1$. Furthermore, ΔT^n_{ik1} must not exceed Θ^n_{i1}, and ΔT^n_{ik2} and ΔT^n_{ik3}, must be zero. In other words

$$\Delta T^n_{ik1} \le \Theta^n_{i1} Y^n_{ik1} \tag{13a}$$

$$\Delta T^n_{ik2} \le \Theta^n_{i2}\left(1 - Y^n_{i(k+1)1}\right) \tag{13b}$$

$$\Delta T^n_{ik3} \le \Theta^n_{i3}\left(1 - Y^n_{i(k+1)1}\right) \tag{13c}$$

A similar argument for the scenario 2 (liquid-to-liquid) gives

$$\Delta T^n_{ik1} \le \Theta^n_{i1}\left(1 - Y^n_{ik3}\right) \tag{14a}$$

$$\Delta T^n_{ik2} \le \Theta^n_{i2}\left(1 - Y^n_{ik3}\right) \tag{14b}$$

$$\Delta T^n_{ik3} \le \Theta^n_{i3} Y^n_{i(k+1)3} \tag{14c}$$

Equation 13a makes Eq. 14a redundant, and Eq. 14c makes Eq. 13c redundant due to Eq. 7. Equations 13b and 14b ensure that ΔT^n_{ik2} is zero, when $Y^n_{i(k+1)1} = 1$ or $Y^n_{ik3} = 1$. However, Eqs. 7, 8a, and 9a imply that $Y^n_{i(k+1)1} + Y^n_{ik3} \le 1$. Therefore, we combine Eqs. 13b and 14b as

$$\Delta T^n_{ik2} \le \Theta^n_{i2}\left(1 - Y^n_{i(k+1)1} - Y^n_{ik3}\right) \tag{15}$$

Note that Eq. 15 is tighter than both Eqs. 13b and 14b together.

For scenario 3 (2-phase-to-2-phase), ΔT^n_{ik1} and ΔT^n_{ik3} must be zero, and, therefore, $\Delta T^n_{ik2} = T^n_{ik} - T^n_{i(k+1)}$. Equations 7, 13a, 14c, and 15 ensure these.

For scenario 4 (gas-to-2-phase), $\Delta T^n_{ik3} = 0$ and $\Delta T^n_{ik1} = T^n_{ik} - DPT^n_i$ must hold. Equations 14c and 7 ensure the former, and the following ensures the latter

$$\Delta T^n_{ik1} + \Theta^n_{i1}\left(2 - Y^n_{ik1} - Y^n_{i(k+1)2}\right) \ge T^n_{ik} - DPT^n_i \tag{16}$$

For scenario 5 (gas-to-liquid), none of ΔT^n_{ik1}, ΔT^n_{ik2}, and ΔT^n_{ik3} needs to be zero, and $\Delta T^n_{ik2} = DPT^n_i - BPT^n_i$. To ensure the latter, we use

$$\Delta T^n_{ik2} \ge \Theta^n_{i2}\left(Y^n_{ik1} + Y^n_{i(k+1)3} - 1\right) \tag{17}$$

For scenario 6 (2-phase-to-liquid), $\Delta T^n_{ik1} = 0$ and $\Delta T^n_{ik3} = BPT^n_i - T^n_{i(k+1)}$ must hold. Eq. 13a ensures the former, and the following ensures the latter

$$\Delta T^n_{ik3} + \Theta^n_{i3}\left(2 - Y^n_{ik2} - Y^n_{i(k+1)3}\right) \ge BPT^n_i - T^n_{i(k+1)} \tag{18}$$

Pursuing similar arguments for scenarios for cold streams, we have

$$\Delta t^n_{jk1} \le \theta^n_1 y^n_{jk1} \tag{19}$$

$$\Delta t^n_{jk3} \le \theta^n_3 y^n_{j(k+1)3} \tag{20}$$

$$\Delta t^n_{jk2} \le \theta^n_2\left(1 - y^n_{jk3} - y^n_{j(k+1)1}\right) \tag{21}$$

$$\Delta t^n_{jk1} + \theta^n_1\left(2 - y^n_{jk1} - y^n_{j(k+1)2}\right) \ge t^n_{jk} - DPT^n_{MR} \tag{22}$$

$$\Delta t^n_{jk2} \ge \theta^n_2\left(y^n_{j(k+1)3} + y^n_{jk1} - 1\right) \tag{23}$$

$$\Delta t^n_{jk3} + \theta^n_3\left(2 - y^n_{jk2} - y^n_{j(k+1)3}\right) \ge BPT^n_{MR} - t^n_{j(k+1)} \tag{24}$$

Energy Balances and HE Areas

For this, we need to model the T-H curve. As remarked earlier, the curve behaves differently for $T \le BPT$, $BPT \le T \le DPT$, and $T \ge DPT$. With no loss of generality, we assume an empirical cubic T-H correlation for each state s as follows

$$\Delta H_{is} = a_{is}\Delta T_{is} + b_{is}[\Delta T_{is}]^2 + c_{is}[\Delta T_{is}]^3$$

$$\Delta h_{js} = a_{MR,s}\Delta t_{js} + b_{MR,s}[\Delta t_{js}]^2 + c_{MR,s}[\Delta t_{js}]^3$$

where, a_{is}, b_{is}, c_{is} ($a_{MR,s}$, $b_{MR,s}$, $c_{MR,s}$) are fitted parameters for state s of stream i (j), ΔH_{is} (Δh_{js}) is the change in the molar enthalpy of stream i (j) in state s, $\Delta T_{i1} = T_i - DPT_i$ for $T_i \geq DPT_i$, $\Delta T_{i2} = DPT_i - T_i$ for $BPT_i \leq T_i \leq DPT_i$, $\Delta T_{i3} = BPT_i - T_i$ for $T_i \leq BPT_i$, $\Delta t_{j1} = t_j - DPT_{MR}$ for $t_j \geq DPT_{MR}$, $\Delta t_{j2} = t_j - BPT_{MR}$ for $BPT_{MR} \leq t_j \leq DPT_{MR}$, $\Delta t_{j3} = BPT_{MR} - t_j$ for $t_j \leq BPT_{MR}$, and T_i (t_j) represents the temperature of stream i (j). Note that a cubic correlation is necessary to capture a possible inflection point in a T-H curve, as we see in Figure 3a–d.

Now, let q^n_{ijk} be the heat duty for HE (i, j, k) for data set n. Using the empirical correlations for the T-H curve, energy balance for each hot (cold) stream i (j) yields

$$\sum_j q^n_{ijk} = M^n_i \sum_s \left[a^n_{is}\Delta T^n_{iks} + b^n_{is}(\Delta T^n_{iks})^2 + c^n_{is}(\Delta T^n_{iks})^3\right] \tag{25a}$$

$$\sum_i q^n_{ijk} = f_j M^n_{MR} \sum_s \left[a^n_{MR,s}\Delta t^n_{jks} + b^n_{MR,s}(\Delta t^n_{jks})^2 + c^n_{MR,s}(\Delta t^n_{jks})^3\right] \tag{25b}$$

Obviously, q^n_{ijk} must be zero, if that HE is not selected, and vice versa. Thus

$$q^{n,L}_{ijk}x_{jk} \leq q^n_{ijk} \leq \min\left[Q^n_i, Q^n_{MR}\right]x_{ijk} \tag{26a,b}$$

where, $q^{n,L}_{ijk}$ is the lower limit on q^n_{ijk}, which a selected HE must satisfy, and

$$Q^n_i = M^n_i \sum_s \left[a^n_{is}\Theta^n_{is} + b^n_{is}(\Theta^n_{is})^2 + c^n_{is}(\Theta^n_{is})^3\right]$$

$$Q^n_{MR} = M^n_{MR} \sum_s \left[a^n_{MR,s}\theta^n_s + b^n_{MR,s}(\theta^n_s)^2 + c^n_{MR,s}(\theta^n_s)^3\right]$$

We should also ensure that the temperature driving forces at the two (hot and cold) ends of the HE exceed the minimum temperature approach (MTA) for every data set n

$$T^n_{ik} - t^n_{jk} \geq MTAx_{ijk} - (TIN^n_i - TIN^n_{MR})(1 - x_{ijk}) \tag{27a}$$

$$T^n_{i(k+1)} - t^n_{j(k+1)} \geq MTAx_{ijk} - (TIN^n_i - TIN^n_{MR})(1 - x_{ijk}) \tag{27b}$$

Now, let A_{ijk} be the area of the HE (i, j, k), which is independent of data sets. Strictly speaking, we must demand

$$A_{ijk} = \frac{q^n_{ijk}}{U^n_{ij}TD^n_{ijk}}$$

where, U^n_{ij} was defined earlier in the assumptions, and TD^n_{ijk} is the temperature driving force for the HE (i, j, k) for the data set n. The strict equality in the aforementioned equation leads to infeasibilities in the optimization problem. Therefore, we allow some flexibility in satisfying the aforementioned across various data sets. We allow the actual area for each exchanger to be within a small neighborhood of A_{ijk} defined by a small prefixed fraction δ_{ijk} as follows.

$$q^n_{ijk} \geq (1 - \delta_{ijk})A_{ijk}U^n_{ij}TD^n_{ijk} \tag{28a}$$

$$q^n_{ijk} \leq (1 + \delta_{ijk})A_{ijk}U^n_{ij}TD^n_{ijk} \tag{28b}$$

Objective Function

Our objective is to match the behavior of the network with that of the real MSHE. One criterion for a good match is the closeness of predicted vs. observed stream outlet temperatures. Recall that we split the MR stream into J cold streams, which do not exist in reality. Thus, their outlet temperatures have no meaning in reality. We only know the outlet temperature of the MR stream, which is the addition of the J cold streams. Computing the outlet temperature of this mixture stream is difficult in our network, because it requires inversion of enthalpy information to temperature information. To avoid this inversion, we measure the closeness of temperatures in the equivalent term of closeness of enthalpies. Even though we could still use temperature closeness for hot streams, we use enthalpy even for them to be consistent. Thus, our objective is to minimize the discrepancies in enthalpy changes for all streams (hot and MR). Even this can be done in several ways. One of them is to minimize the sum of squares of the differences between the observed and predicted enthalpy changes

$$\min \sum_n \left[\sum_i \sqrt{\left(\Delta H^n_i - \sum_j \sum_k q^n_{ijk}\right)^2} + \sqrt{\left(\Delta H^n_{MR} - \sum_i \sum_j \sum_k q^n_{ijk}\right)^2}\right]$$

where, ΔH^n_i and ΔH^n_{MR} are known constants representing the observed changes in the enthalpies of hot stream i and MR in the bundle.

An alternative that avoid the nonlinear functions would be to use absolute, but normalized, differences are follows

$$E^n_i \geq 1 - \left(\sum_j \sum_k q^n_{ijk}\right)/\Delta H^n_i \tag{29a}$$

$$E^n_i \geq \left[\left(\sum_j \sum_k q^n_{ijk}\right)/\Delta H^n_i\right] - 1 \tag{29b}$$

$$E^n_{MR} \geq 1 - \left(\sum_i \sum_j \sum_k q^n_{ijk}\right)/\Delta H^n_{MR} \tag{29c}$$

$$E^n_{MR} \geq \left[\left(\sum_i \sum_j \sum_k q^n_{ijk}\right)/\Delta H^n_{MR}\right] - 1 \tag{29d}$$

In principle, we could minimize the maximum of these errors, but we minimize the sum instead, as that objective function gives better computational performance

$$\min\left[\sum_i \sum_n E^n_i + \sum_n E^n_{MR}\right] \tag{30}$$

This completes our MINLP formulation (F0) that involves Eqs. 1–12, 13a, 14c, and 15–30. After solving the model, we obtain outlet temperatures of all streams from their outlet enthalpies.

Alternate Model Using Disjunctive Programming

The temperature changes in a stage k for a hot (cold) stream in the three states can be also modeled as disjunctions based on different scenarios. As stated before, multiple scenarios exist for a hot (cold) stream in a known sequence, but only one scenario occurs for each HE. Therefore, the disjunctions must define the selection of scenarios, and appropriate propositional logic to maintain their proper sequence. Appendix B gives the details of such a disjunctive model with its convex hull reformulation.[33] It also shows that our proposed formulation (F0) is as tight as the convex hull reformulation.

Solution Strategy

Although unlike simultaneous HENS formulations, we have a linear objective function, it is clear that F0 is a nonconvex MINLP. Therefore, local MINLP solvers cannot guarantee its global solution. The proposed formulation is larger and relatively more complex than the existing HENS formulations due to the presence of phase change. Thus, it is not easy to solve F0 for a real MSHE, even with a few sets of observed data. From our experience, the available commercial solvers such as GAMS/BARON[34] and GAMS/DICOPT[35] fail to yield even a local optimal solution after many hours of CPU time for our proposed formulation. Although DICOPT quickly finds a feasible solution, successive iterations drag on for long. This seems to be due to the MILP master problems, since the original problem has many constraints and binary variables. Moreover, the NLP subproblems often become increasingly infeasible. Then, DICOPT is unable to construct a new linearization, and solution improvement becomes difficult. Thus, we need an efficient algorithm even for getting a local optimal solution to this difficult problem.

Algorithm

A major simplification in our formulation arises from the fact that the objective function involves enthalpy changes only and no HE areas. Thus, the solution would not change, even if Eqs. 28a,b were excluded from the optimization. We could check the feasibilities of areas after the optimization. Because Eqs. 28a,b represent the major nonlinearities in this problem, their elimination reduces the solution time drastically. However, because of the nonconvexity, we need an iterative algorithm that uses a global solver such as BARON to improve the solution quality as much as possible. Therefore, our algorithm (Figure 5) involves solving two MINLP, and one NLP subproblems derived from the parent MINLP (P), which is obtained by removing Eqs. 28a,b from F0.

As the first step, we need a feasible network configuration (x_{ijk}) to begin iterations. This can be readily obtained by selecting some HEs arbitrarily subject to Eqs. 3–6 in P, or by using DICOPT to solve P. We use the latter strategy in the first iteration. However, instead of letting DICOPT reach a

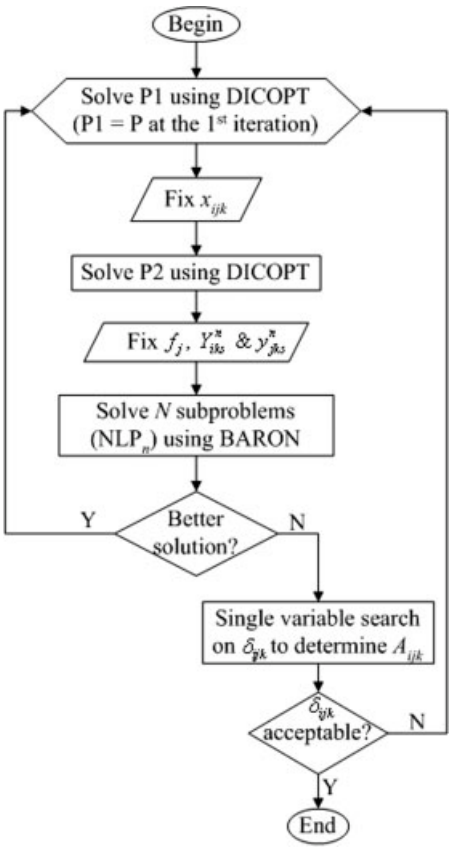

Figure 5. Flow chart of the proposed iterative algorithm.

locally optimal solution, we simply take the best solution after four major iterations. We call this solution S1. In contrast to the first iteration, where we obtain S1 by solving P, we obtain S1 by solving an amended version of P in subsequent iterations. We call this amended version of P as P1, which we obtain by adding several integer cuts to P after the first iteration, or to P1 after the second and subsequent iterations.

Using S1, we fix x_{ijk} in P to obtain an MINLP subproblem (P2) at each iteration. We then solve P2 using DICOPT to find f_j and the stream states (Y^n_{iks} and y^n_{jks}) for all data sets in each HE. We call this solution as S2. We call S* as the best of S1 and S2. Using S*, we fix f_j, Y^n_{iks} and y^n_{jks} in P to obtain N NLP subproblems (NLP_n, $n = 1, 2, \ldots, N$), one for each data set. We solve these N NLPs to global optimality by using BARON, and obtain the values for the continuous variables.

Having, thus, examined a given configuration in some detail, we now eliminate this configuration from subsequent consideration by adding two integer cuts to P1 (or P after the first iteration) as follows

$$\sum_{(i,j,k)\ni[x_{ijk}]=1} x_{ijk} \le \left(\sum_i \sum_j \sum_k [x_{ijk}]\right) - 1 \qquad (31)$$

$$\sum_i \sum_j \sum_k x_{ijk} \le \sum_i \sum_j \sum_k [x_{ijk}] \qquad (32)$$

where, $[x_{ijk}]$ is the fixed value of x_{ijk} used in the current iteration. Eq. 31 ensures that the same set of exchangers is not

used again, and Eq. 32 ensures that the number of exchangers in the network keeps decreasing as iterations proceed.

The algorithm iterates, until the best solution from an iteration cannot be improved in the next iteration. Using the best solution, we then compute heat-transfer areas. Note that the areas can be computed using a rigorous approach, which need not use LMTD. Since the phases are known for the matches, one can use appropriate methods for computing U and driving forces, which fully consider the complexity of the T-H relations. One commonly used approach is to discretize each stream into several segments,[2] and compute the area for each segmented stream. Clearly, for the values ($[q^n_{ijk}]$) of q^n_{ijk} from the best solution, A_{ijk} must satisfy the following (Eqs. 28a,b).

$$\frac{[q^n_{ijk}]}{(1-\delta_{ijk})U^n_{ij}TD^n_{ijk}} \geq A_{ijk} \geq \frac{[q^n_{ijk}]}{(1+\delta_{ijk})U^n_{ij}TD^n_{ijk}} \tag{33}$$

Thus, A_{ijk} must be such that

$$\min_n \left[\frac{[q^n_{ijk}]}{(1-\delta_{ijk})U^n_{ij}TD^n_{ijk}}\right] \geq A_{ijk} \geq \max_n \left[\frac{[q^n_{ijk}]}{(1+\delta_{ijk})U^n_{ij}TD^n_{ijk}}\right] \tag{34a,b}$$

For a given δ_{ijk}, the aforementioned equation gives us an acceptable range of values for A_{ijk}. However, notice that reducing δ_{ijk} will reduce this range and increase our accuracy for energy balance. Therefore, we propose to use a single variable search to obtain the minimum δ_{ijk} that reduces this range to a single value of A_{ijk}. Of course, it is possible that minimum δ_{ijk} is too large to be acceptable. Therefore, if all the minimum δ_{ijk} are acceptably low, then we accept the network solution. If not, then S* does not represent a feasible network. In this case, we return to our algorithm, add an integer cut on x_{ijk} in P to exclude S*, and then repeat our algorithm to identify another network.

We must mention that DICOPT may fail to solve at an iteration due to an infeasible NLP subproblem. We can handle this situation by using the "elastic" formulation recommended in GAMS/DICOPT solver.[35] This involves introducing slack variables for x_{ijk}, Y^n_{iks} and, y^n_{jks}, and adding them to the objective function with a penalty for binary infeasibility.

We now use the aforementioned model and algorithm for a case study involving an existing MCHE in a base-load LNG plant in Qatar to illustrate their efficacy in predicting future operation.

Case Study on LNG

LNG, the cleanest of the fossil fuels, is a fast growing primary energy source for the world today. LNG in global business comes into picture because natural gas transportation has always been a tricky problem. Pipelines are the traditional way of transportation, but they are not always feasible or economical. Pipeline transportation costs more than US$2 per MMBTU of natural gas, and increases approximately proportionately with distance. In fact, subsea lines over 2,000 miles are usually regarded as uneconomic.[36] In addition, there is a greater security risk from pipelines. That is why, nowadays, the option of liquefying and then transporting natural gas as LNG by specially built ships is becoming more popular. When liquefied, the volume of natural gas reduces by a factor of about 600 at room-temperature, which facilitates the bulk transport of natural gas. In fact, this can be viewed as an excellent example of DFL (Design (product) For Logistics[37]). The fast depletion of world's crude oil reserves, high oil prices, concerns and restrictions on CO_2 emission, desire to diversify energy supply, and economical and technological barriers to renewable energy sources are paving the way for ever increasing global demand for LNG. According to IEA World Energy Outlook (2006), the investment for natural gas will equal that for oil (19% of the total energy investment) and the cumulative spending on natural gas supply infrastructure is slated to rise by US$3.9 trillion during 2001–2030, and a lion share of this investment will be attributed to LNG. Recent reductions[38–40] in costs throughout the LNG chain, advances in technology,[39] new-generation LNG tankers,[37] etc., have transformed LNG into an increasingly global energy option, and has established it as the fuel for the future. In 2005, total LNG movement was 188.81 bcm.[41] As an alternate fuel, the demand of LNG is doubling every 10 years. A growth rate of around 6.5% per year[36] is expected for LNG in the near future, which will be the fastest growth for any energy activity or product worldwide.

LNG business has enjoyed high profit margins, because very few countries produce LNG. However, LNG supply chain is highly capital intensive, and new market dynamics such as the emergence of new LNG players, third parties, and customers and increasing spot transactions, etc., are making the LNG industry more vibrant and competitive. For instance, Singapore is in the process of constructing an import terminal and a re-gasification plant, with the intention of becoming a regional hub for natural gas. With the increase in global competition among the LNG producers, the profit margin will not continue to remain high. Moreover, although the cost for producing LNG has reduced by some 40% in the last 20 years, LNG production is still expensive (around 15 US$/bbl oil equivalent or US$2.5 per thousand scf).[36] Liquefaction and transportation costs for LNG represent nearly 85% of the cost of delivering LNG to the customer's jetty. A major part of this cost is attributed to energy consumption in the refrigeration section. Therefore, it is imperative to model MCHE toward the optimization of LNG operations.

To maintain confidentiality, we have scaled all the data (flows, temperatures, etc.). The MCHE (Figure 6) has three bundles (HB, MB, and CB). All three bundles use one MR stream, but with different characteristics (flow rates, compositions, temperatures, etc.). We denote them by MR1, MR2, and MR3, respectively, for HB, MB, and CB. HB and MB have four hot streams each, namely H1 to H4 for HB, and H5 to H8 for MB. CB has only two hot streams, namely H9 and H10.

Due to the extreme temperatures in Qatar, the natural gas feed temperature varies by as much as 20 °C between summer and winter. Therefore, it was important to use the MCHE operational data over the entire year to include the effects of all possible ambient conditions. The LNG plant in Qatar stores historic plant data in DCS (Digital Control System), from which we extracted the data for 1 year. However,

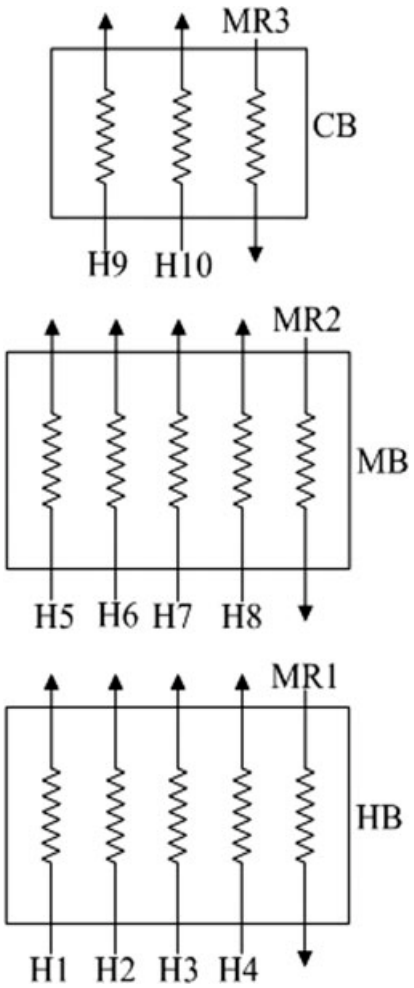

Figure 6. Schematic of the MCHE bundles for the example.

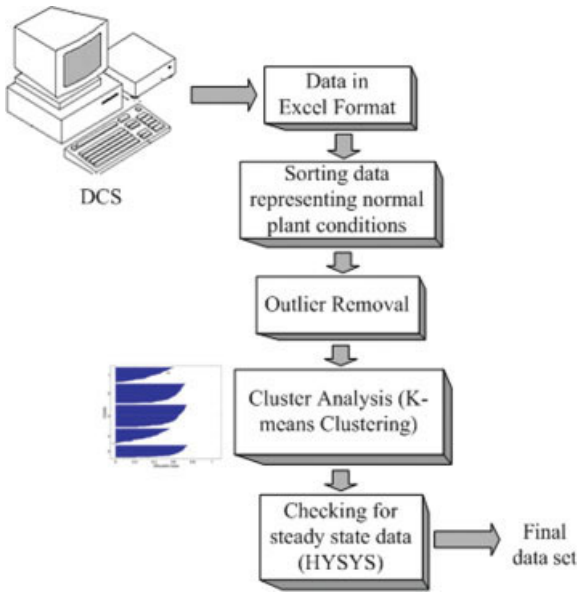

Figure 7. Framework for sorting industrial data.

[Color figure can be viewed in the online issue, which is available at www.interscience.wiley.com.]

as expected with real dynamic plant data, all the operating data were not measured or available for the same time point, which posed a problem. Therefore, our first step was to identify only the most representative and steady-state data. To this end, we used the approach in Figure 7. First, we removed all data sets with missing values. Then, we eliminated the data sets that corresponded to upsets and disruptions in MCHE operation. Given the expected ranges of values for normal operation, we then deleted each data set that involved a variable out of the expected range. We also plotted the data and removed the sets with outliers. Next, we classified all the remaining data sets into groups (or clusters) using the K-means clustering method in the Statistics Toolbox of MATLAB. The K-means method partitions the data sets into N mutually exclusive clusters, and returns a vector of indices indicating the N clusters to which each data set belongs. One advantage of the K-means clustering is that it is specially suited for large amount of data. It creates a single level of clusters rather than a tree structure, and delivers clusters that are as compact and well-separated as possible. We implemented this entire procedure in MATLAB 7.2.0. Using the Silhouette values from the K-means method, we select one data set from each cluster and check for mass

Table 1. Scaled Flow Data (fu) for Model Development

	HB					MB					CB		
Data Set	H1	H2	H3	H4	MR1	H5	H6	H7	H8	MR2	H9	H10	MR3
1	2.569	0.0583	0.7883	2.859	3.706	2.420	0.0583	0.7883	2.859	3.706	2.4783	0.7883	1.840
2	2.464	0.0526	0.6849	2.267	3.003	2.342	0.0526	0.6849	2.267	3.003	2.3946	0.6849	1.736
3	2.330	0.0559	0.6596	2.450	3.160	2.203	0.0559	0.6596	2.450	3.160	2.2589	0.6596	1.709
4	2.320	0.0538	0.6764	2.492	3.219	2.198	0.0538	0.6764	2.492	3.219	2.2518	0.6764	1.727
5	2.439	0.0537	0.7465	2.701	3.504	2.317	0.0537	0.7465	2.701	3.504	2.3707	0.7465	1.803
6	2.463	0.0540	0.7642	2.787	3.608	2.323	0.0540	0.7642	2.787	3.608	2.3770	0.7642	1.822
7	2.448	0.0529	0.7751	2.719	3.552	2.323	0.0529	0.7751	2.719	3.552	2.3759	0.7751	1.833
8	2.734	0.0564	0.8169	3.013	3.892	2.609	0.0564	0.8169	3.013	3.892	2.6654	0.8169	1.878
9	2.689	0.0562	0.7976	2.961	3.818	2.563	0.0562	0.7976	2.961	3.818	2.6192	0.7976	1.858
10	2.435	0.0537	0.8059	2.813	3.680	2.201	0.0537	0.8059	2.813	3.680	2.2547	0.8059	1.868
11	2.323	0.0524	0.8222	2.838	3.722	2.304	0.0524	0.8222	2.838	3.722	2.3564	0.8222	1.878
12	2.426	0.0551	0.7352	2.394	3.184	2.335	0.0551	0.7352	2.394	3.184	2.3901	0.7352	1.793
13	2.464	0.0599	0.7623	2.596	3.416	2.269	0.0599	0.7623	2.596	3.416	2.3289	0.7623	1.823
14	2.391	0.0541	0.8047	2.973	3.838	2.547	0.0541	0.8047	2.973	3.838	2.6011	0.8047	1.866

Table 2. Scaled Inlet Temperature Data (tu) for Model Development

	HB					MB					CB		
Data Set	H1	H2	H3	H4	MR1	H5	H6	H7	H8	MR2	H9	H10	MR3
1	2.350	2.410	2.410	2.420	2.100	2.170	2.120	2.223	2.260	1.471	1.521	1.500	1.141
2	2.350	2.420	2.410	2.423	2.081	2.174	2.100	2.182	2.181	1.466	1.520	1.503	1.127
3	2.380	2.420	2.410	2.410	2.075	2.166	2.100	2.160	2.210	1.489	1.522	1.504	1.129
4	2.390	2.410	2.410	2.410	2.093	2.167	2.110	2.194	2.280	1.506	1.549	1.540	1.153
5	2.355	2.406	2.410	2.410	2.080	2.164	2.104	2.155	2.198	1.497	1.548	1.533	1.140
6	2.340	2.420	2.410	2.410	2.100	2.178	2.127	2.210	2.183	1.485	1.529	1.521	1.127
7	2.389	2.412	2.390	2.417	2.083	2.171	2.103	2.187	2.182	1.502	1.531	1.520	1.156
8	2.362	2.401	2.390	2.410	2.095	2.178	2.115	2.206	2.226	1.499	1.527	1.516	1.160
9	2.392	2.402	2.390	2.409	2.095	2.163	2.115	2.208	2.226	1.487	1.516	1.508	1.156
10	2.368	2.405	2.405	2.420	2.106	2.174	2.116	2.223	2.220	1.496	1.522	1.516	1.156
11	2.339	2.411	2.401	2.416	2.096	2.158	2.116	2.199	2.224	1.517	1.556	1.544	1.164
12	2.340	2.414	2.412	2.428	2.100	2.190	2.124	2.199	2.223	1.491	1.522	1.512	1.181
13	2.346	2.401	2.396	2.413	2.109	2.156	2.119	2.203	2.162	1.507	1.535	1.524	1.137
14	2.330	2.405	2.396	2.411	2.103	2.177	2.113	2.204	2.226	1.519	1.549	1.546	1.154

balance to ensure steady-state validity. We did this by using an in-house HYSYS simulation model for the LNG plant. If a data set does not satisfy the steady-state requirement, then we select another data set nearest to its cluster's center.

For our case study, we identified 798 data sets from 1,462 raw data sets representing 1 year of operation. The K-means method gave us 14 clusters from these 798 data sets. The 14 best data sets (1–14) from these clusters satisfied the steady-state requirement, and were selected for network generation. Tables 1 and 2 present the flow and inlet temperature data for all streams in scaled units (fu for flow and tu for temperature). Table 3 gives the scaled property data (BPT, DPT, etc.), and only the nonzero coefficients in T-H correlations. They are assumed to be constants for all data sets. The coefficients in the T-H correlations are computed by best fitting them against real T-H data for each stream. We obtain these data from HYSYS using Peng Robinson as the fluid package. Note that our proposed expressions for the T-H correlations implicitly ensure that the end points of each region match exactly with the real data. With the aforementioned data, we used a scaled MTA of 0.002 and $q_{ijk}^{n,L} = 0.001$ qu (scaled enthalpy unit), to obtain the best network for each bundle (HB, MB, and CB) individually. We also used $(T_i^{n,L}, t_{MR}^{n,U}) = (2, 2.5)$, (1.3, 2.3), and (1, 2) for HB, MB, and CB, respectively. We solved our model on an AMD Athlon^{TM} 64 $\times$ 2 Dual Core Processor 6000+ 3.00 GHz, 3.00 GB of RAM using BARON v.7.5, and DICOPT with CPLEX v.10.0.1 (MILP solver), and CONOPT v.3 (NLP solver) in GAMS 22.2.

Table 4 gives the model and solution statistics, respectively, for the three bundles. The parent MINLPs (P) for HB and MB have the same numbers of variables (6,987 continuous and 1,408 binary including the slack variables), and constraints (11,937), which are larger than those for CB. CB required the smallest model with 1,637 continuous and 344 binary variables, and 2,571 constraints. The algorithm required one iteration for HB, and two for MB and CB. In each iteration, the solution quality improves significantly each time the binary variables x_{ijk} are fixed after P1, and the model is solved again as P2. For HB, for instance, the best objective value after solving P1 is 18.129. However, after fixing x_{ijk}, and solving P2, the objective value improves significantly to 1.7463. This also holds true for both the iterations for MB and CB. This underlines the usefulness of fixing binary variables successively in our algorithm. One reason behind the improvement in solution quality for P2 could be the reduction in the numbers of nonconvex terms and binary variables as compared to P1. Fixing the network topology naturally makes P2 less complex and easier to solve than P1. Furthermore, note that the best objective value of P2 from DICOPT is either the same as or very close to the total of globally best objective values for NLPs from BARON. The final objective values for HB, MB, and CB are 1.7463, 1.7983, and 3.701, respectively. These can be compared with the upper bounds of 70, 70, and 42 for HB, MB, and CB, respectively, to get an idea of the model's fits to the data. The model solution times for HB, MB, and CB are 336.7, 1601, and 303 CPU s, respectively. Although the model sizes of HB and MB are similar, their solution times are significantly different. One possible explanation is the difficulty introduced by the presence of phase change for

Table 3. Scaled Property Data and Nonzero Coefficients for the Temperature-Enthalpy Correlations

Stream	*DPT*	*BPT*	α	β	a_1	a_2	a_3	b_2	c_2	Max. Error
H1	2.195	1.998	242.70	–	0.65	2.328451	0.80	−1.35810	−1.46210	±4.1%
H2, H6	3.544	2.712	70.900	–	1.00	1.441031	0.90	−0.29660	1.59590	±8.5%
H3, H7	2.400	1.858	173.43	–	0.60	1.493541	0.65	−0.28000	0.01730	±6.2%
H4, H8	2.948	2.400	155.30	–	0.90	0.569857	0.70	2.55670	−1.09420	±3.1%
H5	2.195	1.998	242.70	–	0.65	2.328451	0.80	−1.35810	−10.4600	±6.8%
H9	2.195	1.998	255.50	–	0.65	2.328451	0.80	−1.35810	−10.4600	±6.8%
H10	2.400	1.858	180.30	–	0.60	1.493541	0.65	−0.28000	0.01730	±4.6%
MR1, MR2	2.730	1.474	–	3.15	0.50	1.297005	0.63	1.04860	−0.69610	±5.8%
MR3	2.740	1.474	–	3.15	0.80	2.297000	0.93	1.04860	−0.69600	±5.8%

Table 4. Model and Solution Statistics

MCHE Bundle	Continuous Variables	Binary Variables	Constraints	Non-Zeros	Nonlinear Non-Zeros	Iteration	P1 CPU Time (sec)	P1 Objective Value	P2 CPU Time (sec)	P2 Objective Value	NLP CPU Time (sec)	NLP Objective Value
HB	6987	1408	11937	45075	1120	1	291.14	18.129	34.514	1.7463	11.02	1.7460
MB	6987	1408	11937	45037	1120	1	993.06	3.985	26.764	2.1754	31.30	2.173
						2	500.25*	3.5783	36.389	1.7983	13.52	1.7980
CB	1637	344	2571	8295	280	1	7.828	5.5293	51.326	4.0344	0.950	4.034
						2	233.01	3.7927	9.084	3.701	0.960	3.701

*stopped at maximum time limit of 500 CPU seconds.

some of the hot streams in MB. This is also true for CB in comparison to HB with the additional factor of much smaller model size. Furthermore, DICOPT was not always successful in case of MB. We imposed a limit of 500 CPU s to terminate DICOPT. This limit took effect in the second iteration of MB as shown in Table 4. During iterations, Eq. 32 reduces the search space significantly. It decreases the CPU time for solving P1. For instance, P1 without Eq. 32 does not converge within the specified limit of 500 CPU s in the second iteration for CB. However, with Eq. 32, it converges within 233.01 CPU s. In some instances, it is observed that DICOPT generates better solution for the problem P to kick-start the algorithm, if Eq. 6 is eliminated. Note that this elimination does not result in any infeasible network configuration, since Eq. 6 is originally obtained as a heuristic rule. It is clear that much work is needed to improve the solution algorithm for this difficult nonlinear problem, which we hope to do in near future.

Using the best solutions (Table 4) obtained earlier, we computed δ_{ijk} (and subsequently A_{ijk}) via a single-variable

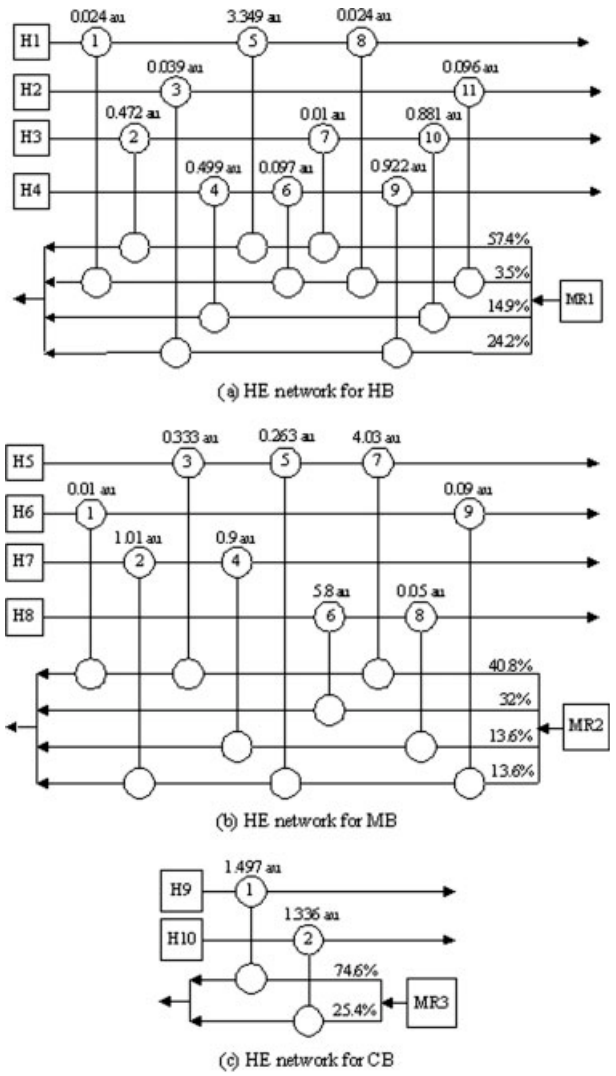

Figure 8. Final HE network of the MCHE bundles for the example.

Table 5. Model Predicted and Actual Outlet Temperatures (tu) for HB

	H1			H2			H3			H4			MR1		
Data Set	Actual	Model	Error (%)	Actual	Model	Error (%)	Actual	Model	Error (%)	Actual	Model	Error (%)	Actual	Model	Error (%)
1	2.110	2.206	−4.55	2.120	2.120	0.00	2.223	2.226	−0.13	2.260	2.259	0.04	2.370	2.463	−3.92
2	2.103	2.213	−5.23	2.100	2.100	0.00	2.182	2.185	−0.14	2.181	2.183	−0.09	2.384	2.427	−1.80
3	2.080	2.206	−6.06	2.100	2.100	0.00	2.160	2.162	−0.09	2.210	2.211	−0.05	2.355	2.425	−2.97
4	2.100	2.212	−5.33	2.110	2.113	−0.14	2.194	2.195	−0.05	2.280	2.280	0.00	2.352	2.507	−6.59
5	2.085	2.199	−5.47	2.104	2.104	0.00	2.155	2.167	−0.56	2.198	2.199	−0.05	2.350	2.478	−5.45
6	2.120	2.209	−4.20	2.127	2.127	0.00	2.210	2.214	−0.18	2.183	2.193	−0.46	2.337	2.335	0.09
7	2.092	2.209	−5.59	2.103	2.103	0.00	2.187	2.189	−0.09	2.182	2.186	−0.18	2.358	2.470	−4.75
8	2.104	2.207	−4.90	2.115	2.115	0.00	2.206	2.208	−0.09	2.226	2.226	0.00	2.361	2.490	−5.46
9	2.104	2.193	−4.23	2.115	2.115	0.00	2.208	2.209	−0.05	2.226	2.226	0.00	2.364	2.491	−5.37
10	2.125	2.219	−4.42	2.116	2.126	−0.47	2.223	2.226	−0.13	2.220	2.220	0.00	2.367	2.471	−4.39
11	2.102	2.195	−4.42	2.116	2.116	0.00	2.199	2.203	−0.18	2.224	2.224	0.00	2.355	2.435	−3.40
12	2.102	2.212	−5.23	2.124	2.124	0.00	2.199	2.202	−0.14	2.223	2.223	0.00	2.343	2.349	−0.26
13	2.110	2.213	−4.88	2.119	2.129	−0.47	2.203	2.206	−0.14	2.162	2.205	−1.99	2.350	2.339	0.47
14	2.10	2.20	−4.47	2.113	2.123	−0.47	2.204	2.207	−0.14	2.226	2.227	−0.04	2.360	2.439	−3.35

Table 6. Model Predicted and Actual Outlet Temperatures (tu) for MB

	H5			H6			H7			H8			MR2		
Data Set	Actual	Model	Error (%)	Actual	Model	Error (%)	Actual	Model	Error (%)	Actual	Model	Error (%)	Actual	Model	Error (%)
1	1.407	1.491	−6.00	1.484	1.491	−0.48	1.488	1.511	−1.57	1.420	1.494	−5.19	2.100	2.089	0.55
2	1.398	1.392	0.43	1.479	1.486	−0.46	1.483	1.490	−0.48	1.421	1.518	−6.85	2.095	2.035	2.86
3	1.425	1.509	−5.90	1.501	1.509	−0.53	1.504	1.511	−0.50	1.439	1.510	−4.93	2.113	2.034	3.73
4	1.469	1.526	−3.88	1.524	1.526	−0.15	1.540	1.540	0.01	1.484	1.527	−2.91	2.104	2.071	1.56
5	1.475	1.517	−2.85	1.516	1.517	−0.07	1.533	1.533	0.01	1.481	1.518	−2.49	2.127	2.034	4.39
6	1.431	1.505	−5.19	1.497	1.505	−0.53	1.501	1.517	−1.03	1.444	1.513	−4.80	2.103	2.033	3.33
7	1.463	1.537	−5.04	1.517	1.522	−0.30	1.520	1.536	−1.05	1.479	1.523	−3.00	2.115	2.037	3.70
8	1.454	1.537	−5.68	1.513	1.519	−0.36	1.516	1.520	−0.26	1.469	1.520	−3.49	2.115	2.055	2.83
9	1.441	1.507	−4.61	1.506	1.507	−0.07	1.508	1.509	−0.04	1.451	1.508	−3.90	2.116	2.083	1.56
10	1.443	1.468	−1.70	1.512	1.516	−0.29	1.516	1.505	0.75	1.455	1.517	−4.26	2.116	2.043	3.44
11	1.478	1.494	−1.10	1.540	1.540	0.00	1.544	1.518	1.68	1.492	1.538	−3.12	2.124	2.048	3.59
12	1.441	1.497	−3.88	1.505	1.511	−0.40	1.512	1.524	−0.80	1.454	1.512	−3.98	2.119	2.061	2.74
13	1.453	1.527	−5.12	1.524	1.527	−0.21	1.524	1.538	−0.89	1.465	1.534	−4.71	2.113	2.064	2.34
14	1.484	1.565	−5.47	1.536	1.539	−0.22	1.546	1.566	−1.31	1.499	1.540	−2.73	2.118	2.061	2.70

Table 7. Model Predicted and Actual Outlet Temperatures (tu) for CB

	H9			H10			MR3		
Data Set	Actual	Model	Error (%)	Actual	Model	Error (%)	Actual	Model	Error (%)
1	1.220	1.296	−6.22	1.205	1.210	−0.46	1.484	1.488	−0.24
2	1.210	1.284	−6.09	1.213	1.213	0.04	1.483	1.487	−0.28
3	1.223	1.269	−3.75	1.213	1.213	0.01	1.511	1.494	1.14
4	1.233	1.282	−4.02	1.216	1.216	−0.02	1.545	1.541	0.24
5	1.210	1.276	−5.44	1.210	1.210	0.00	1.538	1.541	−0.18
6	1.204	1.265	−5.08	1.198	1.198	0.01	1.506	1.518	−0.80
7	1.232	1.283	−4.11	1.206	1.214	−0.67	1.529	1.523	0.39
8	1.225	1.306	−6.60	1.203	1.227	−1.99	1.524	1.517	0.44
9	1.223	1.301	−6.34	1.226	1.226	0.04	1.513	1.501	0.79
10	1.223	1.265	−3.43	1.217	1.221	−0.34	1.514	1.512	0.11
11	1.246	1.279	−2.62	1.226	1.226	0.01	1.553	1.560	−0.43
12	1.229	1.305	−6.14	1.213	1.229	−1.34	1.511	1.510	0.09
13	1.214	1.266	−4.31	1.203	1.203	0.02	1.518	1.526	−0.54
14	1.241	1.300	−4.79	1.217	1.217	0.02	1.554	1.551	0.19

Table 8. Scaled Flow Data (fu) for the Prediction of MCHE Operation

	HB					MB					CB		
Data Set	H1	H2	H3	H4	MR1	H5	H6	H7	H8	MR2	H9	H10	MR3
15	2.675	0.0590	0.8167	2.964	3.842	2.453	0.0590	0.8167	2.964	3.842	2.5120	0.8167	1.951
16	2.447	0.0529	0.7751	2.036	3.869	2.321	0.0529	0.7751	2.036	3.869	2.3739	0.7751	1.936
17	2.390	0.0540	0.8047	2.863	3.729	2.290	0.0540	0.8047	2.863	3.729	2.3440	0.8047	1.972
18	2.451	0.0513	0.7105	2.139	2.903	2.314	0.0513	0.7105	2.139	2.903	2.3653	0.7105	1.841
19	2.431	0.0514	0.7257	2.123	2.903	2.311	0.0514	0.7257	2.123	2.903	2.3624	0.7257	1.893
20	2.482	0.0510	0.6837	2.241	2.976	2.332	0.0510	0.6837	2.241	2.976	2.3830	0.6837	1.918
21	2.448	0.0510	0.7980	2.019	2.770	2.299	0.0510	0.7980	2.019	2.770	2.3500	0.7980	1.924
22	2.440	0.0502	0.6998	2.171	2.924	2.316	0.0502	0.6998	2.171	2.924	2.3662	0.6998	1.969
23	2.448	0.0502	0.7522	2.263	3.072	2.328	0.0502	0.7522	2.263	3.072	2.3782	0.7522	1.961
24	2.393	0.0549	0.7445	3.170	3.970	2.292	0.0549	0.7445	3.170	3.970	2.3469	0.7445	1.965
25	2.395	0.0545	0.7976	2.838	3.696	2.292	0.0545	0.7976	2.838	3.696	2.3465	0.7976	1.975
26	2.431	0.0497	0.6679	2.250	2.969	2.316	0.0497	0.6679	2.250	2.969	2.3657	0.6679	1.989
27	2.451	0.0585	0.7511	3.148	3.956	2.331	0.0585	0.7511	3.148	3.956	2.3895	0.7511	1.942
28	2.461	0.0580	0.6932	3.062	3.808	2.340	0.0580	0.6932	3.062	3.808	2.3980	0.6932	1.859

Table 9. Scaled Inlet Temperature Data (tu) for the Prediction of MCHE Operation

	HB					MB					CB		
Data Set	H1	H2	H3	H4	MR1	H5	H6	H7	H8	MR2	H9	H10	MR3
15	2.343	2.409	2.395	2.414	2.110	2.180	2.118	2.205	2.227	1.450	1.529	1.546	1.134
16	2.339	2.412	2.402	2.417	2.083	2.181	2.103	2.187	2.182	1.446	1.535	1.527	1.129
17	2.331	2.405	2.396	2.411	2.093	2.169	2.113	2.204	2.226	1.421	1.526	1.532	1.134
18	2.341	2.416	2.409	2.423	2.075	2.173	2.095	2.166	2.213	1.446	1.530	1.529	1.127
19	2.342	2.415	2.407	2.421	2.069	2.180	2.089	2.150	2.214	1.434	1.563	1.530	1.131
20	2.345	2.420	2.408	2.421	2.077	2.172	2.097	2.175	2.224	1.481	1.525	1.504	1.148
21	2.347	2.423	2.408	2.421	2.077	2.174	2.092	2.156	2.223	1.498	1.534	1.518	1.142
22	2.341	2.417	2.410	2.423	2.077	2.179	2.097	2.172	2.211	1.479	1.550	1.515	1.189
23	2.345	2.417	2.410	2.423	2.072	2.170	2.092	2.149	2.213	1.491	1.518	1.512	1.173
24	2.340	2.412	2.395	2.411	2.095	2.171	2.115	2.201	2.228	1.489	1.523	1.513	1.186
25	2.337	2.405	2.396	2.411	2.081	2.162	2.101	2.210	2.207	1.501	1.527	1.537	1.190
26	2.344	2.423	2.408	2.421	2.100	2.182	2.101	2.188	2.218	1.472	1.551	1.522	1.182
27	2.341	2.403	2.394	2.409	2.081	2.163	2.101	2.176	2.230	1.501	1.550	1.521	1.188
28	2.340	2.404	2.394	2.409	2.080	2.174	2.100	2.171	2.224	1.508	1.532	1.547	1.159

Table 10. Model Predictions for HB Outlet Temperatures (tu)

	H1			H2			H3			H4			MR1		
Data Set	Observed	Model	Error (%)	Observed	Model	Error (%)	Observed	Model	Error (%)	Observed	Model	Error (%)	Observed	Model	Error (%)
15	2.113	2.213	−4.73	2.118	2.134	−0.76	2.205	2.206	−0.05	2.227	2.240	−0.58	2.360	2.371	−0.47
16	2.092	2.193	−4.83	2.103	2.103	0.00	2.187	2.180	0.32	2.182	2.227	−2.06	2.357	2.367	−0.42
17	2.104	2.197	−4.42	2.113	2.114	−0.05	2.204	2.193	0.50	2.226	2.227	−0.04	2.360	2.364	−0.17
18	2.077	2.184	−5.15	2.095	2.101	−0.29	2.166	2.193	−1.25	2.213	2.205	0.36	2.384	2.383	0.04
19	2.077	2.184	−5.15	2.089	2.095	−0.29	2.150	2.192	−1.95	2.214	2.200	0.63	2.383	2.383	0.00
20	2.098	2.191	−4.43	2.097	2.102	−0.24	2.175	2.187	−0.55	2.224	2.210	0.63	2.383	2.383	0.00
21	2.079	2.184	−5.05	2.092	2.104	−0.57	2.156	2.198	−1.95	2.223	2.203	0.90	2.383	2.386	−0.13
22	2.090	2.186	−4.59	2.097	2.101	−0.19	2.172	2.191	−0.87	2.211	2.208	0.14	2.384	2.382	0.08
23	2.073	2.195	−5.89	2.092	2.096	−0.19	2.149	2.194	−2.09	2.213	2.206	0.32	2.377	2.383	−0.25
24	2.103	2.183	−3.80	2.115	2.115	0.00	2.201	2.179	1.00	2.228	2.234	−0.26	2.355	2.361	−0.25
25	2.093	2.193	−4.78	2.101	2.103	−0.10	2.210	2.186	1.09	2.207	2.220	−0.59	2.352	2.366	−0.60
26	2.110	2.195	−4.03	2.101	2.122	−1.00	2.188	2.199	−0.50	2.218	2.225	−0.32	2.384	2.383	0.04
27	2.083	2.189	−5.09	2.101	2.105	−0.19	2.176	2.172	0.18	2.230	2.225	0.22	2.384	2.362	0.92
28	2.082	2.192	−5.28	2.100	2.105	−0.24	2.171	2.165	0.28	2.224	2.224	0.00	2.346	2.364	−0.77

Table 11. Model Predictions for MB Outlet Temperatures (tu)

	H5			H6			H7			H8			MR2		
Data Set	Observed	Model	Error (%)	Observed	Model	Error (%)	Observed	Model	Error (%)	Observed	Model	Error (%)	Observed	Model	Error (%)
15	1.471	1.533	−4.21	1.487	1.484	0.20	1.546	1.673	−8.21	1.452	1.529	−5.30	2.110	2.152	−1.99
16	1.482	1.472	0.67	1.483	1.472	0.74	1.527	1.616	−5.83	1.448	1.530	−5.66	2.083	2.076	0.34
17	1.476	1.453	1.56	1.504	1.451	3.52	1.532	1.538	−0.39	1.443	1.507	−4.44	2.093	2.083	0.48
18	1.481	1.513	−2.16	1.519	1.475	2.90	1.529	1.591	−4.07	1.444	1.496	−3.60	2.075	2.133	−2.80
19	1.477	1.504	−1.83	1.526	1.464	4.06	1.530	1.612	−5.36	1.493	1.485	0.54	2.069	2.120	−2.46
20	1.470	1.536	−4.49	1.501	1.507	−0.40	1.504	1.540	−2.39	1.451	1.530	−5.44	2.077	2.152	−3.61
21	1.454	1.560	−7.29	1.515	1.524	−0.59	1.518	1.669	−9.95	1.457	1.534	−5.28	2.077	2.145	−3.27
22	1.481	1.535	−3.65	1.520	1.504	1.05	1.515	1.655	−9.24	1.493	1.523	−2.01	2.077	2.148	−3.42
23	1.478	1.539	−4.13	1.514	1.515	−0.07	1.512	1.660	−9.79	1.475	1.534	−4.00	2.072	2.137	−3.14
24	1.454	1.509	−3.78	1.511	1.514	−0.20	1.513	1.654	−9.32	1.464	1.572	−7.38	2.095	2.120	−1.19
25	1.469	1.562	−6.33	1.520	1.527	−0.46	1.537	1.680	−9.30	1.484	1.564	−5.39	2.081	2.149	−3.27
26	1.439	1.527	−6.12	1.514	1.497	1.12	1.522	1.590	−4.47	1.462	1.524	−4.24	2.100	2.154	−2.57
27	1.452	1.523	−4.89	1.524	1.529	−0.33	1.521	1.596	−4.93	1.473	1.581	−7.33	2.081	2.103	−1.06
28	1.475	1.533	−3.93	1.536	1.536	0.00	1.547	1.693	−9.44	1.501	1.589	−5.86	2.080	2.112	−1.54

Table 12. Model Predictions for CB Outlet Temperatures (tu)

	H9			H10			MR3		
Data Set	Observed	Model	Error (%)	Observed	Model	Error (%)	Observed	Model	Error (%)
15	1.224	1.293	−5.64	1.196	1.206	−0.84	1.486	1.485	0.07
16	1.221	1.282	−5.00	1.208	1.193	1.24	1.491	1.489	0.13
17	1.243	1.278	−2.82	1.202	1.201	0.08	1.511	1.482	1.92
18	1.212	1.286	−6.11	1.231	1.182	3.98	1.550	1.490	3.87
19	1.199	1.293	−7.84	1.209	1.185	1.99	1.540	1.514	1.69
20	1.226	1.293	−5.46	1.207	1.186	1.74	1.511	1.475	2.38
21	1.217	1.289	−5.92	1.219	1.185	2.79	1.532	1.484	3.13
22	1.215	1.319	−8.56	1.212	1.224	−0.99	1.519	1.500	1.25
23	1.224	1.303	−6.45	1.217	1.222	−0.41	1.511	1.475	2.38
24	1.229	1.310	−6.59	1.220	1.231	−0.90	1.514	1.480	2.25
25	1.210	1.313	−8.51	1.225	1.244	−1.55	1.553	1.492	3.93
26	1.204	1.314	−9.14	1.208	1.210	−0.17	1.513	1.498	0.99
27	1.232	1.322	−7.31	1.203	1.235	−2.66	1.520	1.507	0.86
28	1.225	1.307	−6.69	1.217	1.203	1.15	1.548	1.499	3.17

search based on Eqs. 34a,b. Interestingly, the maximum value of δ_{ijk} across was 27.2%. While this may seem like a large discrepancy between the areas predicted by the various data sets, considering the inherent inaccuracies in heat transfer coefficient correlations, we judged this to be acceptable. Furthermore, as we show later, the predictive performance of our models was quite good even with the above range of δ_{ijk} values. Therefore, we did not repeat our algorithm to obtain smaller values for δ_{ijk}. Figures 8a–c show the complete network configuration for the MCHE with appropriate HE areas and MR split fractions. Following the standard representation for HEN from the literature, each HE is shown as two circles connected by a line. For example, the HE network for CB (Figure 8c) has two HEs. HE 1 has an area of 1.497 au (scaled area unit), and involves H9 as the hot stream, and 74.6% MR as the cold stream. The individual bundle networks require 11, 9, and 2 HEs for HB, MB, and CB, respectively. HB and MB networks require more HEs than the number of hot streams. Post solution, we computed the MR temperature out of each bundle by mixing the cold streams. Tables 5–7 show the percent deviations of stream outlet temperatures predicted by the model from those observed in the data. The average absolute deviations for HB, MB, and CB are 1.77%, 2.39%, and 1.90%, with maximum absolute deviations being 6.59%, 6.85%, and 6.60%, respectively. We observe that the deviations are larger for the streams involving phase change. This is probably due to the approximate T-H correlations for the 2-phase regions.

We also tried to solve this case study using the disjunctive programming model (DP) presented in Appendix B using both DICOPT and BARON. However, no feasible solution was obtained, even after 5,000 CPU s for any bundle. This demonstrates the need for and utility of the specially tailored model and algorithm presented in this article.

Prediction of MCHE Operation

To assess the predictive ability of our model and approach, we extracted 14 data sets (15–28) representing the MCHE operation in another year using the same approach described previously for the data sets 1–14. Tables 8 and 9 present the flow rates and inlet temperatures, respectively, for all streams in scaled units for data sets 15–28. Using these inlet conditions and our derived HE networks (Figure 8a–c) for the MCHE bundles, we predicted the performance of the MCHE for sets 15–28. As shown in Tables 10–12, our networks are able to match the observed stream outlet temperatures within $\pm 10\%$. In absolute terms, these represent deviations of at most 3–4 °C in stream outlet temperatures. This demonstrates our model's ability to predict the MCHE operation in real life.

Conclusions

We presented an MINLP approach to model and predict the operation of complex, proprietary, multistream heat exchangers such as those found in LNG plants and other cryogenic applications. Our approach employed the novel idea of representing a multistream heat exchanger as a network of 2-stream HEs. We demonstrated the success of our approach using the data from a real MCHE (Main Cryogenic Heat Exchanger) in an existing LNG plant in Qatar. Our proposed MINLP model is nonconvex and unsolvable using standard commercial solvers such as DICOPT and BARON, hence, we developed an iterative decomposition algorithm to obtain very good solutions with reasonable effort.

This work represents a critical step toward integrated optimization of plants involving complex multistream heat exchangers. It also enables the simulation of such exchangers in commercial simulators such as HYSYS and AspenPlus by means of simple 2-stream exchangers. Finally, it provided the first step toward an extension of the traditional HEN methodology to include phase changes of mixtures, which we hope to report in very near future.

We must highlight the need for properly preprocessing and scaling the real operational data, as most plant data will not represent perfect steady states. For this, we developed a systematic procedure, which is useful in other applications as well. While an artificial neural network is a viable alternative approach for the problem discussed in this article, we found that it failed to compete with our proposed approach. For instance, its performance in predicting operation away from the training conditions was poor.

Acknowledgments

The authors would like to acknowledge the financial support for this work from the National University of Singapore (NUS), Qatar University, and Qatargas Operating Company, Ltd. The work was done under a NUS-QU collaborative research project 05017P with additional support from Qatargas. The authors are also grateful to various people of Qatargas Operating Company, Ltd. and Air Products for their help, support, comments, and suggestions. We would also like to thank Prof I M Mujtaba of the University of Bradford for suggesting us to evaluate the effectiveness of an artificial neural network for this problem.

Notation

Indices

i = hot stream
j = cold stream
k = stage
n = data set
s = state (liquid, gas, 2-phase) of a stream
l = scenario

Parameters

α, β = parameters for film heat-transfer coefficient
δ_{ijk} = flexibility index for fitting HE areas in the network
Θ_{is}^{n} = maximum possible temperature change at state s for hot stream i, and data set n
θ_{s}^{n} = maximum possible temperature change at state s for MR for data set n
a, b, c = parameters in temperature-enthalpy correlation
BPT_{i}^{n} = bubble-point temperature of hot stream i for data set n
BPT_{MR}^{n} = bubble-point temperature for MR for data set n
DPT_{i}^{n} = dew-point temperature of hot stream i for data set n
DPT_{MR}^{n} = dew-point temperature of MR for data set n
ΔH_{i}^{n} = observed change in enthalpy of hot stream i for data set n
ΔH_{MR}^{n} = observed change in enthalpy of MR for data set n
M_{i}^{n} = molar flow rate of hot stream i for data set n
M_{MR}^{n} = molar flow rate of MR for data set n
MTA = minimum temperature approach
$q_{ijk}^{n,L}$ = lower bound on the heat duty for data set n if HE (i, j, k) exists
TIN_{i}^{n} = inlet temperature of hot stream i for data set n
TIN_{MR}^{n} = inlet temperature of MR for data set n
$TOUT_{i}^{n}$ = observed outlet temperature of hot stream i for data set n

$TOUT_i^n$ = observed outlet temperature of MR for data set n
$T_i^{n,L}$ = lower bound for the temperature of hot streami i for data set n
$t_{MR}^{n,U}$ = upper bound for the temperature of MR for data set n

Binary variables

x_{ijk} = 1 if HE (i,j,k) exists
Y_{iks}^n = 1 if a hot stream i enters a stage k in a state s for data set n
y_{jks}^n = 1 if a cold stream j leaves a stage k in a state s for data set n
Z_{ikl}^n = 1 if a scenario l is selected for a hot stream i at stage k for data set n
z_{jkl}^n = 1 if a scenario l is selected for a cold stream j at stage k for data set n

Boolean variables

BY_{ikl}^n = true if a scenario l is selected for a hot stream i at stage k for data set n
By_{jkl}^n = true if a scenario l is selected for a cold stream j at stage k for data set n

Continuous variables

A_{ijk} = area of the HE (i, j, k)
$E_i^n (E_{MR}^n)$ = normalized errors for hot stream i (MR)
f_j = split fraction of MR to create cold stream j
TD_{ijk}^n = appropriate temperature driving force for the HE (i, j, k)
q_{ijk}^n = heat load in a HE (i, j, k) for data set n
T_{ik}^n = temperature of hot stream i when it enters stage k for data set n
t_{jk}^n = temperature of cold stream j when it leaves stage k for data set n
ΔT_{iks}^n = temperature change that occurs in state s of hot stream i at stage k for data set n
Δt_{jks}^n = temperature change that occurs in state s of cold stream j at stage k for data set n
U_{ij}^n = overall heat transfer coefficient for (i, j) match for data set n

Literature Cited

1. Bach W, Foerg W, Steinbauer M, Stockmann R, Voggenreiter F. Spiral wound heat exchangers for LNG baseload plants. Presented in the 13th International Conference of Exhibition on Liquefied Natural Gas; May 14–17, 2001; Seoul, Korea.
2. Lee GC, Smith R, Zhu XX. Optimal synthesis of mixed-refrigerant systems for low temperature processes. *Ind Eng Chem Res*. 2002; 41:5016–5028.
3. Flynn TM. *Cryogenic Engineering*. 2nd ed. New York: Marcel Dekker; 2005.
4. Demetri EP. A general method for the analysis of compact multifluid heat exchangers. Presented in the American Society of Mechanical Engineers, Paper 72-HT.14; 1973.
5. Picón-Núñez M, Polley GT, Medina-Flores M. Thermal design of multi-stream heat exchangers. *Appl Thermal Eng*. 2002;22:1643–1660.
6. Yee TF, Grossmann IE, Kravanja Z. Simultaneous optimization models for heat integration-I. Area and energy targeting and modeling of multi-stream exchangers. *Comp Chem Eng*. 1990;14:1151–1164.
7. Zargarzadeh M, Karimi IA, Alfadala HE. Olexan: a tool for online exergy analysis. Presented in ESCAPE17; May 27–30, 2007; Bucharest, Romania.
8. Dubar C, Forcey T, Humphreys V, Schmidt H. A competive offshore LNG scheme utilising a gravity base structure and improved nitrogen cycles. In: *Proceedings of the LNG 12, Institute of Gas Technology*. May 4–7, 1998; Perth, Australia.
9. Liu H, You L. Characteristics and applications of the cold heat exergy of liquefied natural gas. *Energy Conv Manage*. 1999;40: 1515–1525.
10. Kanoğlu M. Exergy analysis of multistage cascade refrigeration cycle used for natural gas liquefaction. *Int J Energy Res*. 2002;26:763–774.
11. Remeljej CW, Hoadley AFA. An exergy analysis of small-scale liquefied natural gas (LNG) liquefaction processes. *Energy*. 2006;31: 2005–2019.
12. Aspelund A, Berstad DO, Gundersen T. An extended pinch analysis and design procedure utilizing pressure based exergy for subambient cooling. *Appl Therm Eng*. 2007;27:2633–2649.
13. Kotas TJ. *The Exergy Method of Thermal Plant Analysis*. Florida: Krieger Publishing Company; 1995.
14. Smith R. *Chemical Process Design and Integration*. NJ: John Wiley; 2005.
15. Vaidyaraman S, Maranas CD. Synthesis of mixed refrigerant cascade cycles. *Chem Eng Commun*. 2002;189:1057–1078.
16. Del Nogal FL, Kim J, Perry SJ, Smith R. Integrated approach for the design of refrigeration and power systems. Presented at 6th Topical Conference on Natural Gas Utilization, AIChE Annual Spring National Meeting, Florida; 2006.
17. Reneume JM, Niclout N. MINLP optimization of plate fin heat exchangers. *Chem Biochem Eng Quart*. 2003;17(1):65–76.
18. Zhu XX, Pua LM. Compact heat exchangers and enhancement technology for the process industry. In: Shah RK, ed. New York: Begell House, Inc; 2001:127–134.
19. Abadzic EE, Scholz HW. Coiled tubular heat exchangers. In: *Advances in cryogenic engineering*. New York: Plenum Press; 1973:42–51.
20. Fredheim AO. Thermal design of coil-wound LNG heat exchangers Shell side heat transfer and pressure drop. University of Trondheim, Norwegian Institute of Technology; 1994. PhD Thesis.
21. Hasan MMF, Alfadala HE, Karimi IA, Grootjans H. Modeling and simulation of main cryogenic heat exchanger in an LNG plant. Presented at the AIChE Annual Meeting, Nov. 12–17, 2006; San Francisco, CA.
22. Hasan MMF, Karimi IA, Alfadala HE, Grootjans H. Modeling and simulation of main cryogenic heat exchanger in a base-load liquefied natural gas plant. In: *Proceedings of the 17th European Symposium on Computer Aided Process Engineering- ESCAPE17*. 2007;219–224.
23. Gundersen T, Naess L. The synthesis of cost optimal heat exchanger networks. An industrial review of the state of the art. *Comp Chem Eng*. 1988;6:503–530.
24. Furman KC, Sahinidis NV. A critical review and annotated bibliography for heat exchanger network synthesis in the 20th century. *Ind Eng Chem Res*. 2002;40:2335–2370.
25. Yee TF, Grossmann IE. Simultaneous optimization models for heat integration-II. Heat exchanger network synthesis. *Comp Chem Eng*. 1990;14:1165–1184.
26. Ciric AR, Floudas CA. Heat exchanger network synthesis without decomposition. *Comp Chem Eng*. 1991;15:385–396.
27. Ponce-Ortega JM, Jiménez-Gutiérrez A, Grossmann IE. Optimal synthesis of HE networks involving isothermal process streams. *Comp Chem Eng*. 2008;32:1918–1942.
28. Hasan MMF, Karimi IA, Alfadala HE. Modeling phase change in heat exchanger network synthesis. Presented in ESCAPE18; June 1–4, 2008; Lyon, France.
29. Kern DQ. *Process Heat Transfer*. New York: McGraw-Hill; 1950.
30. Holman JP. *Heat Transfer*. 8th ed. New York: McGraw-Hill, Inc; 1997.
31. Neeraas BO, Freheim AO, Aunan B. Experimental data and model for heat transfer, in liquid falling film flow on shell-side, for spiral-wound LNG heat exchanger. *Int J Heat Mass Transfer*. 2004;47: 3565–3572.
32. Bays GS, McAdams WH. Heat transfer coefficients in falling film heaters, streamline flow. *Ind Eng Chem*. 1937:29(11):1240–1246.
33. Raman R, Grossmann IE. Modelling and computational techniques for logic based integer programming. *Comp Chem Eng*. 1994;18(7): 563–578.
34. Sahinidis N, Tawarmalani M. BARON. In: *GAMS: the Solver Manuals*. GAMS Development Corporation; 2005. http://www.gams.com/dd/docs/solvers/baron.pdf.
35. Grossmann IE, Viswanathan J, Vecchietti A, Raman R, Kalvelagen E. DICOPT. In: *GAMS: the Solver Manuals*. GAMS Development Corporation; 2005. http://www.gams.com/dd/docs/solvers/dicopt.pdf.
36. Thomas S, Dawe RA. Review of ways to transport natural gas energy from countries which do not need the gas for domestic use. *Energy*. 2003;28:1461–1477.

37. Lee HL. Design for Supply Chain Management: Concepts and Examples. In: Sarin RK. *Perspectives in operations management: essays in honor of Elwood S. Buffa*. Boston: Kluwer Academic Publishers; 1993:44–66.
38. Morita K, Ueda T, Nagasaka S. Study of changes in patterns of LNG tanker operation. In: summary report of the findings of the "Study of changes in patterns of LNG tanker operation." *IEEJ*. December 2003.
39. Kjärstad J, Johnsson F. Prospects of the European gas market. *Energy Policy*. 2007;35:869–888.
40. Michel V, Marie-Françoise C, Thierry L. World LNG prospects: favorable parameters for a new growth era. Presented in the 18th Congress of World Energy Council; October 2001; Buenos Aires, Argentina.
41. BP Statistical Review of World Energy; June 2006.

Appendix A: Proof for the Two Redundant Equations

Using Eq. 7a, we can write $Y^n_{ik1} + Y^n_{ik2} + Y^n_{ik3} = Y^n_{i(k+1)1} + Y^n_{i(k+1)2} + Y^n_{i(k+1)3}$. Applying Eq. 9a, we get $Y^n_{ik1} + Y^n_{ik2} \geq Y^n_{i(k+1)1} + Y^n_{i(k+1)2}$. This makes $Y^n_{ik1} + Y^n_{ik2} \geq Y^n_{i(k+1)2}$ redundant.

Similarly, $Y^n_{i(k+1)1} + Y^n_{i(k+1)2} + Y^n_{i(k+1)3} = Y^n_{ik1} + Y^n_{ik2} + Y^n_{ik3}$. Applying Eq. 8a, we get $Y^n_{i(k+1)2} + Y^n_{i(k+1)3} \geq Y^n_{ik2} + Y^n_{ik3}$. This makes $Y^n_{i(k+1)2} + Y^n_{i(k+1)3} \geq Y^n_{ik2}$ redundant.

Appendix B: The Disjunctive Programming Model

Six scenarios ($l = 1, \ldots, 6$) are possible for the entrance and exit states of a stream in a stage. Let $BY^n_{iks} = \{True, False\}$ and $By^n_{jkt} = \{True, False\}$ be the Boolean variables to select scenarios for hot and cold streams (i and j), respectively, in stage k. A disjunction is selected, when the corresponding Boolean variable is *True*. The following disjunctions and propositional logic model the temperature changes for a hot (cold) stream $i(j)$ at stage k.

Hot streams

$$\begin{bmatrix} BY^n_{ik1} \\ \Delta T^n_{ik1} \leq T^n_{ik} - T^n_{i(k+1)} \\ \Delta T^n_{ik2} \leq 0 \\ \Delta T^n_{ik3} \leq 0 \\ DPT^n_i \leq T^n_{ik} \leq TIN^n_i \\ DPT^n_i \leq T^n_{i(k+1)} \leq TIN^n_i \end{bmatrix} \vee \begin{bmatrix} BY^n_{ik2} \\ \Delta T^n_{ik1} \leq T^n_{ik} - DPT^n_i \\ \Delta T^n_{ik2} \leq DPT^n_i - T^n_{i(k+1)} \\ \Delta T^n_{ik3} \leq 0 \\ DPT^n_i \leq T^n_{ik} \leq TIN^n_i \\ BPT^n_i \leq T^n_{i(k+1)} \leq DPT^n_i \end{bmatrix} \vee \begin{bmatrix} BY^n_{ik3} \\ \Delta T^n_{ik1} \leq T^n_{ik} - DPT^n_i \\ \Delta T^n_{ik2} \leq DPT^n_i - BPT^n_i \\ \Delta T^n_{ik3} \leq BPT^n_i - T^n_{i(k+1)} \\ DPT^n_i \leq T^n_{ik} \leq TIN^n_i \\ T^{n,L}_i \leq T^n_{i(k+1)} \leq BPT^n_i \end{bmatrix} \vee$$
$$\begin{bmatrix} BY^n_{ik4} \\ \Delta T^n_{ik1} \leq 0 \\ \Delta T^n_{ik2} \leq T^n_{ik} - T^n_{i(k+1)} \\ \Delta T^n_{ik3} \leq 0 \\ BPT^n_i \leq T^n_{ik} \leq DPT^n_i \\ BPT^n_i \leq T_{i(k+1)n} \leq DPT^n_i \end{bmatrix} \vee \begin{bmatrix} BY^n_{ik5} \\ \Delta T^n_{ik1} \leq 0 \\ \Delta T^n_{ik2} \leq T^n_{ik} - BPT^n_i \\ \Delta T^n_{ik3} \leq BPT^n_i - T^n_{i(k+1)} \\ BPT^n_i \leq T^n_{ik} \leq DPT^n_i \\ T^{n,L}_i \leq T_{i(k+1)n} \leq BPT^n_i \end{bmatrix} \vee \begin{bmatrix} BY^n_{ik6} \\ \Delta T^n_{ik1} \leq 0 \\ \Delta T^n_{ik2} \leq 0 \\ \Delta T^n_{ik3} \leq T^n_{ik} - T^n_{i(k+1)} \\ T^{n,L}_i \leq T^n_{ik} \leq BPT^n_i \\ T^{n,L}_i \leq T^n_{i(k+1)} \leq BPT^n_i \end{bmatrix} \quad \text{(DH)}$$

Cold streams

$$\begin{bmatrix} By^n_{jk1} \\ \Delta t^n_{jk1} \leq t^n_{jk} - t^n_{j(k+1)} \\ \Delta t^n_{jk2} \leq 0 \\ \Delta t^n_{jk3} \leq 0 \\ TIN^n_{MR} \leq t^n_{jk} \leq BPT^n_{MR} \\ TIN^n_{MR} \leq t^n_{j(k+1)} \leq BPT^n_{MR} \end{bmatrix} \vee \begin{bmatrix} By^n_{jk2} \\ \Delta t^n_{jk1} \leq BPT^n_{MR} - t^n_{j(k+1)} \\ \Delta t^n_{jk2} \leq t^n_{jk} - BPT^n_{MR} \\ \Delta t^n_{jk3} \leq 0 \\ BPT^n_{MR} \leq t^n_{jk} \leq DPT^n_{MR} \\ TIN^n_{MR} \leq t^n_{j(k+1)} \leq BPT^n_{MR} \end{bmatrix} \vee \begin{bmatrix} By^n_{jk3} \\ \Delta t^n_{jk1} \leq BPT^n_{MR} - t^n_{j(k+1)} \\ \Delta t^n_{jk2} \leq DPT^n_{MR} - BPT^n_{MR} \\ \Delta t^n_{jk3} \leq t^n_{jk} - DPT^n_{MR} \\ DPT^n_{MR} \leq t^n_{jk} \leq t^{n,U}_{MR} \\ TIN^n_{MR} \leq t^n_{j(k+1)} \leq BPT^n_{MR} \end{bmatrix} \vee$$
$$\begin{bmatrix} By^n_{jk4} \\ \Delta t^n_{jk1} \leq 0 \\ \Delta t^n_{jk2} \leq t^n_{jk} - t^n_{j(k+1)} \\ \Delta t^n_{jk3} \leq 0 \\ BPT^n_{MR} \leq t^n_{jk} \leq DPT^n_{MR} \\ BPT^n_{MR} \leq t^n_{j(k+1)} \leq DPT^n_{MR} \end{bmatrix} \vee \begin{bmatrix} By^n_{jk5} \\ \Delta t^n_{jk1} \leq 0 \\ \Delta t^n_{jk2} \leq DPT^n_{MR} - t^n_{j(k+1)} \\ \Delta t^n_{jk3} \leq t^n_{jk} - DPT^n_{MR} \\ DPT^n_{MR} \leq t^n_{jk} \leq t^{n,U}_{MR} \\ BPT^n_{MR} \leq t^n_{j(k+1)} \leq DPT^n_{MR} \end{bmatrix} \vee \begin{bmatrix} By^n_{jk6} \\ \Delta t^n_{jk1} \leq 0 \\ \Delta t^n_{jk2} \leq 0 \\ \Delta t^n_{jk3} \leq t^n_{jk} - t^n_{j(k+1)} \\ DPT^n_{MR} \leq t^n_{jk} \leq t^{n,U}_{MR} \\ DPT^n_{MR} \leq t^n_{j(k+1)} \leq t^{n,U}_{MR} \end{bmatrix} \quad \text{(DC)}$$

The propositional logic for a hot stream i is

$$BY^n_{ik1} \Rightarrow BY^n_{i(k+1)1} \vee BY^n_{i(k+1)2} \vee BY^n_{i(k+1)3}$$

$$BY^n_{ik2} \Rightarrow BY^n_{i(k+1)4} \vee BY^n_{i(k+1)5}$$

$$BY^n_{ik3} \Rightarrow BY^n_{i(k+1)6}$$

$$BY^n_{ik4} \Rightarrow BY^n_{i(k+1)4} \vee BY^n_{i(k+1)5}$$

$$BY^n_{ik5} \Rightarrow BY^n_{i(k+1)6}$$

$$BY^n_{ik6} \Rightarrow BY^n_{i(k+1)6}$$

$$BY^n_{i(k+1)1} \Rightarrow BY^n_{ik1}$$

$$BY^n_{i(k+1)2} \Rightarrow BY^n_{ik1}$$

$$BY^n_{i(k+1)3} \Rightarrow BY^n_{ik1}$$

$$BY^n_{i(k+1)4} \Rightarrow BY^n_{ik2} \vee BY^n_{ik4}$$

$$BY^n_{i(k+1)5} \Rightarrow BY^n_{ik2} \vee BY^n_{ik4}$$

$$BY^n_{i(k+1)6} \Rightarrow BY^n_{ik3} \vee BY^n_{ik5} \vee BY^n_{ik6}$$

The propositional logic for a cold stream j is

$$By^n_{j(k+1)1} \Rightarrow By^n_{jk1} \vee By^n_{jk2} \vee By^n_{jk3}$$

$$By^n_{j(k+1)2} \Rightarrow By^n_{jk4} \vee By^n_{jk5}$$

$$By^n_{j(k+1)3} \Rightarrow By^n_{jk6}$$

$$By^n_{j(k+1)4} \Rightarrow By^n_{jk4} \vee By^n_{jk5}$$

$$By^n_{j(k+1)5} \Rightarrow By^n_{jk6}$$

$$By^n_{j(k+1)6} \Rightarrow By^n_{jk6}$$

$$By^n_{jk1} \Rightarrow By^n_{j(k+1)1}$$

$$By^n_{jk2} \Rightarrow By^n_{j(k+1)1}$$

$$By^n_{jk3} \Rightarrow By^n_{j(k+1)1}$$

$$By^n_{jk4} \Rightarrow By^n_{j(k+1)2} \vee By^n_{j(k+1)4}$$

$$By^n_{jk5} \Rightarrow By^n_{j(k+1)2} \vee By^n_{j(k+1)4}$$

$$By^n_{jk6} \Rightarrow By^n_{j(k+1)3} \vee By^n_{j(k+1)5} \vee By^n_{j(k+1)6}$$

A Convex hull formulation of the disjunctions

Let us replace BY^n_{ikl} and By^n_{jkl} by binary variables Z^n_{ikl} and z^n_{jkl}, respectively. Let us also introduce temperature variables TI^n_{ikl}, and TO^n_{ikl}. Since the formulation (C0) of the convex hull of the disjunctions is similar for hot and cold streams, we show it for the hot streams only

$$\sum_l Z^n_{ikl} = 1 \qquad \text{(C0)}$$

$$T_{ikn} = \sum_l TI^n_{ikl}$$

$$T_{i(k+1)n} = \sum_l TO^n_{ikl}$$

$$\Delta T^n_{ik1} \leq TI^n_{ik1} + TI^n_{ik2} + TI^n_{ik3} - TO^n_{ik1} - DPT^n_i Z^n_{ik2} - DPT^n_i Z^n_{ik3}$$

$$\Delta T^n_{ik2} \leq DPT^n_i Z^n_{ik2} + DPT^n_i Z^n_{ik3} + TI^n_{ik4} + TI^n_{ik5} - TO^n_{ik2} - BPT^n_i Z^n_{ik3} - TO^n_{ik4} - BPT^n_i Z^n_{ik5}$$

$$\Delta T^n_{ik3} \leq BPT^n_i Z^n_{ik3} + BPT^n_i Z^n_{ik5} + TI^n_{ik6} - TO^n_{ik3} - TO^n_{ik5} - TO^n_{ik6}$$

$$DPT^n_i Z^n_{ik1} \leq TI^n_{ik1} \leq T^{n,U}_i Z^n_{ik1}$$

$$DPT^n_i Z^n_{ik2} \leq TI^n_{ik2} \leq T^{n,U}_i Z^n_{ik2}$$

$$DPT^n_i Z^n_{ik3} \leq TI^n_{ik3} \leq T^{n,U}_i Z^n_{ik3}$$

$$BPT^n_i Z^n_{ik4} \leq TI^n_{ik4} \leq DPT^n_i Z^n_{ik4}$$

$$BPT^n_i Z^n_{ik5} \leq TI^n_{ik5} \leq DPT^n_i Z^n_{ik5}$$

$$T^{n,L}_i Z^n_{ik6} \leq TI^n_{ik6} \leq BPT^n_i Z^n_{ik6}$$

$$DPT^n_i Z^n_{ik1} \leq TO^n_{ik1} \leq T^{n,U}_i Z^n_{ik1}$$

$$BPT^n_i Z^n_{ik2} \leq TO^n_{ik2} \leq DPT^n_i Z^n_{ik2}$$

$$T^{n,L}_i Z^n_{ik3} \leq TO^n_{ik3} \leq BPT^n_i Z^n_{ik3}$$

$$BPT^n_i Z^n_{ik4} \leq TO^n_{ik4} \leq DPT^n_i Z^n_{ik4}$$

$$T^{n,L}_i Z^n_{ik5} \leq TO^n_{ik5} \leq BPT^n_i Z^n_{ik5}$$

$$T^{n,L}_i Z^n_{ik6} \leq TO^n_{ik6} \leq BPT^n_i Z^n_{ik6}$$

Moreover, the propositions for the hot streams can be transformed into the following linear constraints

$$Z^n_{i(k+1)1} + Z^n_{i(k+1)2} + Z^n_{i(k+1)3} \geq Z^n_{ik1}$$

$$Z^n_{i(k+1)4} + Z^n_{i(k+1)5} \geq Z^n_{ik2}$$

$$Z^n_{i(k+1)6} \geq Z^n_{ik3}$$

$$Z^n_{i(k+1)4} + Z^n_{i(k+1)5} \geq Z^n_{ik4}$$

$$Z^n_{i(k+1)6} \geq Z^n_{ik5}$$

$$Z^n_{i(k+1)6} \geq Z^n_{ik6}$$

$$Z^n_{ik1} \geq Z^n_{i(k+1)1}$$

$$Z^n_{ik1} \geq Z^n_{i(k+1)2}$$

$$Z_{ikn1} \geq Z^n_{i(k+1)3}$$

$$Z^n_{ik2} + Z^n_{ik4} \geq Z^n_{i(k+1)4}$$

$$Z^n_{ik2} + Z^n_{ik4} \geq Z^n_{i(k+1)5}$$

$$Z^n_{ik3} + Z^n_{ik5} + Z^n_{ik6} \geq Z^n_{i(k+1)6}$$

Tightness of the formulation (F0) and (C0)

Again, we show this only for the hot streams. From the convex hull formulation, the following relaxations for ΔT^n_{iks} can be derived

$$\Delta T^n_{ik1} \leq \left(TIN^n_i - DPT^n_i\right)\left(Z^n_{ik1} + Z^n_{ik2} + Z^n_{ik3}\right) \quad \text{(DPR1)}$$

$$\Delta T^n_{ik2} \leq \left(DPT^n_i - BPT^n_i\right)\left(Z^n_{ik2} + Z^n_{ik3} + Z^n_{ik4} + Z^n_{ik5}\right) \quad \text{(DPR2)}$$

$$\Delta T^n_{ik3} \leq \left(BPT^n_i - T^{n,L}_i\right)\left(Z^n_{ik3} + Z^n_{ik5} + Z^n_{ik6}\right) \quad \text{(DPR3)}$$

In order to prove that F0 also provides equally tight relaxations for ΔT^n_{iks} as C0, we now show that Eqs. DPR1–R3 and linear constraints for the logic propositions can be derived from F0.

The relations between Z^n_{ikl} and Y^n_{iks} can be written as: $Z^n_{ik1} = Y^n_{ik1}Y^n_{i(k+1)1}, Z^n_{ik2} = Y^n_{ik1}Y^n_{i(k+1)2}, Z^n_{ik3} = Y^n_{ik1}Y^n_{i(k+1)3}, Z^n_{ik4} = Y^n_{ik2}Y^n_{i(k+1)2}, Z^n_{ik5} = Y^n_{ik2}Y^n_{i(k+1)3}, Z^n_{ik6} = Y^n_{ik3}Y^n_{i(k+1)3}$. Therefore, $Z^n_{ik1} + Z^n_{ik2} + Z^n_{ik3} = Y^n_{ik1}\left(Y^n_{i(k+1)1} + Y^n_{i(k+1)2} + Y^n_{i(k+1)3}\right)$. By using, $\sum_s Y^n_{iks} = 1$ we get

$$Z^n_{ik1} + Z^n_{ik2} + Z^n_{ik3} = Y^n_{ik1} \quad \text{(A1)}$$

Similarly

$$Z^n_{ik3} + Z^n_{ik5} + Z^n_{ik6} = Y^n_{i(k+1)3} \quad \text{(A2)}$$

$$Z^n_{ik2} + Z^n_{ik3} + Z^n_{ik4} + Z^n_{ik5} = \left(1 - Y^n_{i(k+1)1}\right)\left(1 - Y^n_{ik3}\right) \quad \text{(A3)}$$

From A3, we get the following three equations

$$Z^n_{ik2} + Z^n_{ik3} + Z^n_{ik4} + Z^n_{ik5} \leq \left(1 - Y^n_{i(k+1)1}\right) \quad \text{(A4)}$$

$$Z^n_{ik2} + Z^n_{ik3} + Z^n_{ik4} + Z^n_{ik5} \leq \left(1 - Y^n_{ik3}\right) \quad \text{(A5)}$$

$$Z^n_{ik2} + Z^n_{ik3} + Z^n_{ik4} + Z^n_{ik5} \geq \left(1 - Y^n_{i(k+1)1} - Y^n_{ik3}\right) \quad \text{(A6)}$$

Now, using Eq. 13a and A1, we obtain $\Delta T^n_{ik1} \leq \left(TIN^n_i - DPT^n_i\right)\left(Z^n_{ik1} + Z^n_{ik2} + Z^n_{ik3}\right)$. Furthermore, using Eq. 14c and A2, we obtain $\Delta T^n_{ik3} \leq \left(BPT^n_i - T^{n,L}_i\right)\left(Z^n_{ik3} + Z^n_{ik5} + Z^n_{ik6}\right)$. Lastly, using Eq. 15 and A6, we obtain $\Delta T^n_{ik2} \leq \left(DPT^n_i - BPT^n_i\right)\left(Z^n_{ik2} + Z^n_{ik3} + Z^n_{ik4} + Z^n_{ik5}\right)$.

Similarly, we can derive the relaxations for cold streams and prove that F0 is as tight as the convex hull formulation of the disjunctive model.

Constraints for the logic propositions from F0

Using the relations between Z^n_{ikl} and Y^n_{iks}, we obtain $Y^n_{i(k+1)1} \geq Z^n_{ik1}, Y^n_{i(k+1)2} \geq Z^n_{ik2}, Y^n_{i(k+1)2} \geq Z^n_{ik4}, Y^n_{i(k+1)3} \geq Z^n_{ik3}, Y^n_{i(k+1)3} \geq Z^n_{ik5}$. Now, from Eq. A1, $Z^n_{i(k+1)1} + Z^n_{i(k+1)2} + Z^n_{i(k+1)3} = Y^n_{i(k+1)1}$. Therefore, $Z^n_{i(k+1)1} + Z^n_{i(k+1)2} + Z^n_{i(k+1)3} \geq Z^n_{ik1}$.

Moreover, $Z^n_{i(k+1)4} + Z^n_{i(k+1)5} = Y^n_{i(k+1)2}(Y^n_{i(k+2)2} + Y^n_{i(k+2)3})$. This can be also written as $Z^n_{i(k+1)4} + Z^n_{i(k+1)5} \geq \left(Y^n_{i(k+1)2}\right)^2 = Y^n_{i(k+1)2}$, since $Y^n_{i(k+2)2} + Y^n_{i(k+2)3} \geq Y^n_{i(k+2)2}$. Therefore, we obtain $Z^n_{i(k+1)4} + Z^n_{i(k+1)5} \geq Z^n_{ik2}$ and $Z^n_{i(k+1)4} + Z^n_{i(k+1)5} \geq Z^n_{ik4}$.

Using Eq. 9a and $Z^n_{ik6} = Y^n_{ik3}Y^n_{i(k+1)3}$, we obtain $Z^n_{ik6} \geq \left(Y^n_{ik3}\right)^2 = Y^n_{ik3}$ or $Z^n_{i(k+1)6} \geq Y^n_{i(k+1)3}$. Now, using the aforementioned relations developed so far, it is trivial to show that $Z^n_{i(k+1)6} \geq Z^n_{ik3}$, $Z^n_{i(k+1)6} \geq Z^n_{ik5}$. Combining Eq. 9a and $Y^n_{ik3} \geq Z^n_{ik6}$, we get $Y^n_{i(k+1)3} \geq Z^n_{ik6}$. Hence, $Z^n_{i(k+1)6} \geq Z^n_{ik6}$.

The relations between Z^n_{ikl} and Y^n_{iks} also imply that $Z^n_{i(k+1)1} = Y^n_{i(k+1)1}Y^n_{i(k+2)1}$. Therefore, $Y^n_{i(k+1)1} \geq Z^n_{i(k+1)1}$. Similarly, $Y^n_{i(k+1)1} \geq Z^n_{i(k+1)2}$ and $Y^n_{i(k+1)1} \geq Z^n_{i(k+1)3}$. Using Eq. 8a and $Z^n_{ik1} = Y^n_{ik1}Y^n_{i(k+1)1}$, we obtain $Z^n_{ik1} \geq \left(Y^n_{i(k+1)1}\right)^2$ or $Z^n_{ik1} \geq Y^n_{i(k+1)1}$. It is now trivial to show that $Z^n_{ik1} \geq Z^n_{i(k+1)1}, Z^n_{ik1} \geq Z^n_{i(k+1)2}$ and $Z^n_{ik1} \geq Z^n_{i(k+1)3}$.

From the relations between Z^n_{ikl} and Y^n_{iks}, we get $Z^n_{ik2} + Z^n_{ik4} = (Y^n_{ik1} + Y^n_{ik2})Y^n_{i(k+1)2}$. However, $Y^n_{ik1} + Y^n_{ik2} \geq Y^n_{i(k+1)2}$. Therefore, $Z^n_{ik2} + Z^n_{ik4} \geq \left(Y^n_{i(k+1)2}\right)^2 = Y^n_{i(k+1)2}$. By definition, $Y^n_{i(k+1)2} \geq Z^n_{i(k+1)4}$ and $Y^n_{i(k+1)2} \geq Z^n_{i(k+1)5}$. Hence, $Z^n_{ik2} + Z^n_{ik4} \geq Z^n_{i(k+1)4}$ and $Z^n_{ik2} + Z^n_{ik4} \geq Z^n_{i(k+1)5}$.

Last, $Z^n_{ik3} + Z^n_{ik5} + Z^n_{ik5} - Z^n_{i(k+1)6} = Y^n_{i(k+1)3}(1 - Y^n_{i(k+2)3})$ since Eq. A2 holds true and $Z^n_{i(k+1)6} = Y^n_{i(k+1)3}Y^n_{i(k+2)3}$. Since for any value of $Y^n_{i(k+1)3}$ and $Y^n_{i(k+2)3}$, $Y^n_{i(k+1)3}(1 - Y^n_{i(k+2)3}) \geq 0$, therefore, $Z^n_{ik3} + Z^n_{ik5} + Z^n_{ik5} \geq Z^n_{i(k+1)6}$.

Manuscript received Mar. 28, 2008, and revision received Sept. 3, 2008.